JCI The Journal of Clinical Investigation

Ribosomal S6 protein kinase 4 promotes radioresistance in esophageal squamous cell carcinoma

Mingyang Li, … , Jian Zhang, Zhe Wang

J Clin Invest. 2020. https://doi.org/10.1172/JCI134930.

Research In-Press Preview Oncology

Graphical abstract

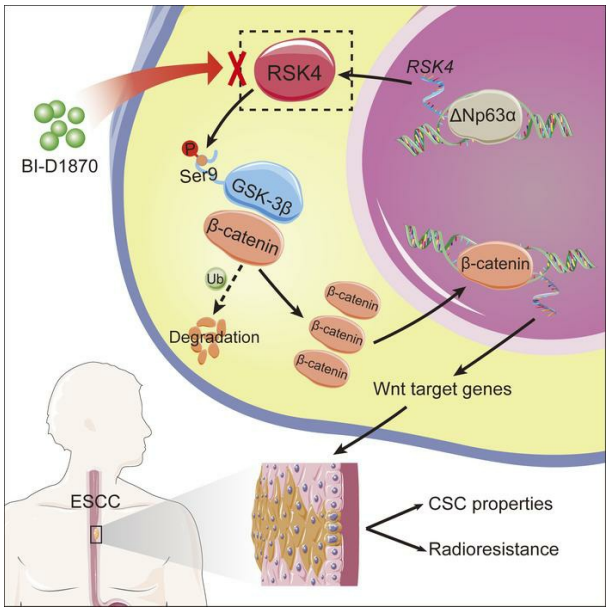

Ribosomal S6 protein kinase 4 promotes radioresistance in esophageal squamous cell carcinoma

Ming-Yang Li[1], Lin-Ni Fan[1], Dong-Hui Han[2], Zhou Yu[1], Jing Ma[1], Yi-Xiong Liu[1], Pei-Feng Li[1], Dan-Hui Zhao[1], Jia Chai[1], Lei Jiang[3], Shi-Liang Li[3], Juan-Juan Xiao[4], Qiu-Hong Duan[5], Jing Ye[1], Mei Shi[6], Yong-Zhan Nie[7], Kai-Chun Wu[7], Dezhong Joshua Liao[8], Yu Shi[9], Yan Wang[9], Qing-Guo Yan[1], Shuang-Ping Guo[1], Xiu-Wu Bian[9], Feng Zhu[4,5,*], Jian Zhang[10,11,*] and Zhe Wang[1,*]

[1]State Key Laboratory of Cancer Biology, Department of Pathology, Xijing Hospital and School of Basic Medicine, Fourth Military Medical University, Xi'an, China

[2]Department of Urology, Xijing Hospital, Fourth Military Medical University, Xi'an, China

[3]Shanghai Key Laboratory of New Drug Design, State Key Laboratory of Bioreactor Engineering, School of Pharmacy, East China University of Science and Technology, Shanghai, China

[4]Cancer Research Institute, The Affiliated Hospital of Guilin Medical University, Guilin, China

[5]Department of Biochemistry and Molecular Biology, School of Basic Medicine, Huazhong University of Science and Technology, Wuhan, China

[6]Department of Radiation Oncology, Xijing Hospital, Fourth Military Medical University, Xi'an, China

[7]State Key Laboratory of Cancer Biology, National Clinical Research Center for Digestive Diseases, Xijing Hospital, Fourth Military Medical University, Xi'an, China

[8]Department of Pathology, the Second Hospital, Guizhou University of Traditional Chinese Medicine, Guiyang, China

[9]Institute of Pathology and Southwest Cancer Center, Southwest Hospital, Third Military Medical University, Chongqing, China

[10]State Key Laboratory of Cancer Biology, Department of Biochemistry and Molecular Biology, School of Basic Medicine, Fourth Military Medical University, Xi'an, China

[11]Key Laboratory of Gastrointestinal Pharmacology of Chinese Materia Medica of the State Administration of Traditional Chinese Medicine, School of Pharmacy, Fourth Military Medical University, Xi'an, China

[*]Corresponding authors:

Zhe Wang, State Key Laboratory of Cancer Biology, Department of Pathology, Xijing Hospital and School of Basic Medicine, Fourth Military Medical University, 169 Changle West Road, Xi'an 710032, China, Phone: 86.29.8471.0422, E-mail: zhwang@fmmu.edu.cn; Jian Zhang, State Key Laboratory of Cancer Biology, Department of Biochemistry and Molecular Biology, School of Basic Medicine and Key Laboratory of Gastrointestinal Pharmacology of Chinese Materia Medica of the State Administration of Traditional Chinese Medicine, School of Pharmacy, Fourth Military Medical University, 169 Changle West Road, Xi'an 710032, China, Phone: 86.29.8471.2325, E-mail: biozhangj@fmmu.edu.cn; and Feng Zhu, Cancer Research

Institute, The Affiliated Hospital of Guilin Medical University, 15 Lequn Road, Guilin 541000, China, Phone: 86.773.286.1220, E-mail: fengzhu@hust.edu.cn.

Conflict of interest: The authors have declared that no conflict of interest exists.

Abstract

Esophageal squamous cell carcinoma (ESCC) is one of the most aggressive cancers and is highly resistant to current treatments. ESCC harbors a subpopulation of cells exhibiting cancer stem-like cell (CSC) properties that contribute to therapeutic resistance including radioresistance, but the molecular mechanisms in ESCC CSCs are currently unknown. Here, we report that ribosomal S6 protein kinase 4 (RSK4) plays a pivotal role in promoting CSC properties and radioresistance in ESCC. RSK4 was highly expressed in ESCC CSCs and associated with radioresistance and poor survival in ESCC patients. RSK4 was found to be a direct downstream transcriptional target of ΔNp63α, the main p63 isoform, which is frequently amplified in ESCC. RSK4 activated the β-catenin signaling pathway through direct phosphorylation of GSK-3β Ser9. Pharmacologic inhibition of RSK4 effectively reduced CSC properties and improves radiosensitivity in both nude mice and patient-derived xenograft models. Collectively, our results strongly suggest that the ΔNp63α-RSK4-GSK-3β axis plays a key role in driving CSC properties and radioresistance in ESCC, indicating that RSK4 is a promising therapeutic target for ESCC treatment.

Introduction

Esophageal cancer is one of the most frequently occurring cancers and ranks as the seventh leading cause of cancer-related mortality worldwide. Esophageal squamous cell carcinoma (ESCC) is the most common histological type of esophageal malignancy and has a higher incidence in developing nations (1), with more than half of ESCC cases occurring in China (2). Despite intensive clinical efforts using multiple therapeutic approaches, patients with ESCC still face a poor prognosis, which has not significantly improved in recent decades (3). The treatment of choice for locally advanced ESCC is neoadjuvant chemoradiation followed by radical surgery. Unfortunately, more than 50% of ESCC cases do not respond adequately and most patients die from recurrent cancer (4). ESCC possesses a subpopulation of cells exhibiting cancer stem-like cell (CSC) properties, which are known to have a high tumorigenic potential and resistance to conventional anticancer therapy and are responsible for the intractable features of ESCC (5, 6). Increasing evidence indicates that CSCs contribute to radioresistance, which could result in radiation treatment failure of ESCC (7, 8). Therefore, targeting CSCs may be promising for developing novel combination modalities and overcoming the radiation resistance of ESCC.

p90 ribosomal S6 kinases (RSKs) are a family of serine-threonine kinases involved in the Ras–mitogen-activated protein kinase (MAPK) pathway. This family consists of four members in humans, RSKs 1-4, along with two structurally related homologues, mitogen- and stress-activated kinase-1 (MSK1) and MSK2 (9). RSKs phosphorylate

many cytosolic and nuclear targets and are integrally linked to a variety of physiological processes, including cell-cycle progression and proliferation, cell growth and protein synthesis, cell migration and cell survival (10). With regard to the role of different RSKs in cancer, it is generally believed that RSK1 and RSK2 promote cancer cell growth, survival and motility (11, 12), whereas RSK3 is downregulated in breast tumors (13) and ovarian cancer (14). RSK4, which was first identified as an X-linked gene in patients with mental retardation, is most abundant in the fetal and adult kidney, brain and thyroid gland (15). Functional characterization analysis shows that RSK4 is constitutively active under serum-starved conditions and independent of 3-phosphoinositide-dependent protein kinase-1 (PDK1) for phosphorylation, whereas other RSKs are inactive due to their requirement for growth factors (16), indicating that RSK4 is functionally distinct from the other RSKs. Compared to the more in-depth research on the other RSKs in the field of cancer, there have been limited and conflicting reports describing the role of RSK4 in different cancer types (17-25). Using a tissue microarray (TMA) containing 20 kinds of human tumors and corresponding normal tissues, we found that RSK4 protein is highly expressed in renal cell carcinoma (RCC) and ESCC. We previously reported that RSK4 is overexpressed in RCC and enhances the invasive and metastatic ability of RCC cells by regulating the CSC marker CD44 (23). In this study, we expand on our previous studies and determine whether RSK4 plays a pathophysiological role in ESCC and CSCs.

Recent genomic analysis has revealed that p63, a p53-related transcriptional factor, is a major oncogenic protein in esophageal cancer; the gene locus is frequently

amplified in ESCC and its expression in ESCC is significantly higher than that in non-tumor tissues (26). *TP63* contains two different promoters that drive two distinct isoform classes: with or without the N-terminal transactivation domain, TAp63 and ΔNp63, respectively. In addition, both TAp63 and ΔNp63 have three variants with different C-termini (α, β, and γ) generated by alternative splicing (27). ΔNp63 and TAp63 show very different expression patterns, depending on the source of cell lines and tissues (28). ΔNp63α is the main p63 isoform expressed in ESCC (29) and plays an important role in maintaining the properties of CSCs (30), but the relationship between p63 and RSK4 remains to be clarified. In this study, we sought to determine whether the ΔNp63α-RSK4 axis plays a role in establishing CSC properties and radioresistance in ESCC, to define the downstream effector genes and pathways controlled by these factors, and to test the rationale for RSK4 as a therapeutic target in this disease.

Results

RSK4 is highly expressed in ESCC CSCs and is associated with the radioresistance and poor survival of ESCC patients

In a TMA containing 20 kinds of human tumors and corresponding normal tissues, immunohistochemical (IHC) staining showed that the RSK4 protein level was significantly reduced in stomach and testis cancer but highly expressed in kidney and esophageal cancer compared with their corresponding non-tumor tissues

(Supplementary Figure 1A and Supplementary Table 1). In esophageal cancer**,** RSK4 protein was highly expressed in ESCC rather than esophageal adenocarcinoma **(Figure 1A and Supplementary Figure 1A).** In 30 paired ESCC and adjacent non-tumor tissues, the *RPS6KA6* (encoding RSK4) mRNA and RSK4 protein levels were also much higher in ESCC than in normal tissues **(Figure 1B, 1C and Supplementary Figure 1B)**. This result was further confirmed by IHC analyses with 87 paired ESCC and adjacent non-tumor tissues **(Figure 1D)**. However, the mRNA levels of the other 2 RSK members, *RPS6KA1* (encoding RSK1) and *RPS6KA3* (encoding RSK2), showed no significant difference. The mRNA level of *RPS6KA2* (encoding RSK3) was much lower in ESCC than in normal tissues **(Supplementary Figure 1C)**. We next employed IHC analysis to examine the prognostic significance of RSK4 expression in clinical tumor samples from cohorts of ESCC patients. Importantly, compared to low RSK4 expression, high expression of RSK4 was correlated with poorer overall survival (OS) and progression-free survival (PFS) of ESCC patients and more aggressive tumor behaviors, including lymph node metastasis and vascular invasion (**Figure 1E, Supplementary Figure 1D and Supplementary Table 2)**, with similar results found in The Cancer Genome Atlas (TCGA) cohort **(Supplementary Figure 1E)**. In addition, the mRNA level of *RPS6KA6* in Grade 2 and Grade 3 cases was higher than those in Grade 1 cases in ESCC **(Supplementary Figure 1F)**. Multivariate Cox regression analysis further indicated RSK4 expression as a potential independent prognostic marker for OS and PFS in ESCC patients **(Supplementary Table 3).**

Surprisingly, we found high RSK4 protein levels in the basal layer of esophageal

epithelia that decrease progressively in the suprabasal and superficial cell compartments with cellular differentiation **(Figure 1D)**, suggesting that RSK4 may be involved in the stemness properties of esophageal epithelia. In ESCC tissues, RSK4 expression was positively correlated with ALDH1, an ESCC CSC marker that we previously identified (31) **(Figure 1F and 1G)**. In addition, the mRNA level of *RPS6KA6* was positively correlated with *ALDH1A1* in the TCGA ESCC cohort **(Supplementary Figure 1G)**. Sphere formation is well established to enrich CSCs on the basis of their self-renewing capacity (32). Similar to other ESCC CSC markers (6), including CD90, CD271, ABCG2, BMI-1, NANOG, OCT4 and SOX2, RSK4 expression was increased in the spheres of ESCC cell line TE10 compared with the corresponding adherent cells, and elevated RSK4 was also observed in $CD90^+$ or $CD271^+$ cell populations compared with $CD90^-$ or $CD271^-$ cell subsets **(Figure 1H and Supplementary Figure 1H)**, suggesting that RSK4 is enriched in ESCC CSCs.

In 10 advanced ESCC patients treated with definitive radiotherapy, RSK4 expression after radiotherapy was significantly higher than that before treatment, which was consistent with the upregulation of CSC marker ALDH1 expression after radiotherapy **(Figure 2A).** A positive correlation between RSK4 and ALDH1 expression was found **(Figure 2B)**, suggesting that RSK4 activation is induced by irradiation and may be involved in CSC-mediated radioresistance. In an enlarged ESCC radiotherapy cohort of 148 patients, patients with high RSK4 expression were significantly associated with radiotherapy resistance; that is, the higher the expression level of RSK4 is, the lower the complete response rate **(Figure 2C)**. Moreover, patients with high RSK4 expression

levels had much worse PFS than those with low RSK4 expression levels **(Figure 2D)**. In summary, RSK4 is specifically upregulated in ESCC CSCs and is linked with radioresistance and poor prognosis in ESCC patients, especially patients undergoing radiotherapy.

RSK4 promotes the CSC properties and radioresistance of ESCC cells

To investigate the biological effects of RSK4 in ESCC, we determined *RPS6KA6* mRNA and RSK4 protein levels in four ESCC cell lines **(Supplementary Figure 2A)** and found that RSK4 expression was higher in the ESCC cell line TE10 and lower in ECA109. Therefore, we generated a stable RSK4-overexpressing clone of ECA109 cells along with stable RSK4-knockdown clones of TE10 cells, as confirmed by real-time PCR and Western blotting **(Supplementary Figure 2B)**. The sphere formation ability was increased in RSK4-overexpressing ECA109 cells but decreased in RSK4-knockdown TE10 cells **(Figure 3A)**. According to flow cytometry and Western blotting, RSK4 overexpression enhanced, while RSK4 knockdown decreased, ALDH activity and the percentage of $CD90^+$ cells as well as the protein levels of CD271, ABCG2, BMI-1, NANOG, OCT4 and SOX2 **(Figure 3B, 3C and Supplementary Figure 2C)**. Limiting dilution analysis (33) of xenografted tumors developed from different numbers of injected cells showed that RSK4 overexpression increased the tumorigenic capacity of ESCC cells, whereas RSK4 knockdown had the opposite effect **(Figure 3D)**. To elucidate the role of RSK4 in ESCC CSC maintenance, we examined the effects of RSK4 knockdown on ESCC CSC proliferation. ESCC CSCs ($CD90^+$ subpopulations)

transfected with shRSK4 proliferated at a lower rate than control cells. In contrast, identical shRSK4 had little effect on matched non-stem ESCC cells ($CD90^-$ subpopulations) (**Supplementary Figure 2D)**. These data suggest that RSK4 exclusively promotes ESCC CSC growth, thereby maintaining the CSC properties of ESCC cells.

With regard to the association between RSK4 and radioresistance, RSK4 overexpression in ESCC cells significantly increased their colony forming ability and decreased caspase-3 activity after irradiation, whereas RSK4 knockdown decreased the colony forming ability of ESCC cells and increased caspase-3 activity after irradiation **(Figure 3E, 3F and Supplementary Figure 2E).** Although irradiation damages tumor cells through several mechanisms, irradiation kills cancer cells primarily through DNA damage. Thus, DNA damage checkpoint responses play essential roles in cellular radiosensitivity (34). The activating phosphorylation of checkpoint proteins ATM and CHK2 induced by irradiation was significantly increased in RSK4-overexpressing ECA109 cells but decreased in RSK4-knockdown TE10 cells **(Figure 3G)**, indicating that RSK4 promotes checkpoint activation in response to DNA damage. The primary downstream effect of checkpoint activation is to induce cell-cycle arrest to repair damaged DNA (35). We then used the comet assay to measure the efficiency of DNA repair after inducing DNA damage with irradiation. RSK4-overexpressing ECA109 cells repaired the DNA damage more efficiently than control cells, as indicated by decreased DNA content in the comet tail 6 h after irradiation, whereas RSK4 knockdown had the opposite effect **(Supplementary Figure 2F)**. This result was

further confirmed by assessing the dynamic changes in γ-H2AX levels after irradiation **(Figure 3H)**. Altogether, these results suggest that RSK4 promotes DNA damage checkpoint responses and DNA damage repair to obtain radioresistance of ESCC cells.

RSK4 is a direct transcriptional target of ΔNp63α in ESCC

To determine the regulation mechanism of RSK4 in ESCC, we performed a transcription factor prediction analysis and noticed one potential binding site of p63 on the *RPS6KA6* gene promoter **(Figure 4A)**. Moreover, *Rps6ka6* is a leading downregulated gene according to RNA sequencing profiling of *Tp63* null squamous epithelia **(Supplementary Figure 3A).** Considering that RSK4 and ΔNp63 protein were highly coexpressed in the basal layer and progressively decreased in the suprabasal and superficial cell compartments with cellular differentiation in esophageal epithelia **(Figure 4B)**, that their mRNA levels were positively correlated in esophagus mucosa in the Genotype-Tissue Expression (GTEx) cohort **(Figure 4C)**, and that the *Rps6ka6* mRNA levels were dramatically decreased in squamous epithelium of *Tp63* knockout mice **(Supplementary Figure 3B)** and in p63 knockdown keratinocytes/ squamous cell carcinoma (SCC) cell lines **(Supplementary Figure 3C)**, we surmised that ΔNp63 transcriptionally regulated RSK4 expression in ESCC. However, the mRNA expression of other RSK family members, including *RPS6KA1*, *RPS6KA3*, *RPS6KA2*, *RPS6KA5* (encoding MSK1) and *RPS6KA4* (encoding MSK2), did not show any appreciable difference under p63 depletion **(Supplementary Figure 3B, 3C)**. As previously reported (36), ΔNp63α was the dominant isoform expressed in ESCC

(Supplementary Figure 3D). Real-time PCR analysis of 30 paired ESCC specimens showed a dramatic upregulation of *ΔNp63* mRNA expression in tumors compared to normal tissues **(Supplementary Figure 3E)**, in accordance with the TCGA database **(Supplementary Figure 3F)**. In ESCC tissues, ΔNp63 expression was positively correlated with RSK4 expression at both the mRNA and protein levels **(Figure 4D, 4E and Supplementary Figure 3G)**, and similar results were obtained from IHC staining of 215 ESCC samples **(Figure 4F)** and in the Gene Expression Omnibus (GEO) cohort **(Supplementary Figure 3H)**. As previously reported (36, 37), ESCC patients with high ΔNp63 protein levels had worse OS and PFS than their low-expression counterparts **(Supplementary Figure 3I)**.

Western blot assays showed that RSK4 expression, but not that of its sibling RSK2, which has been reported to be oncogenic in SCC (12), was positively correlated with ΔNp63 expression in ESCC cell lines **(Supplementary Figure 3J)**. Moreover, ΔNp63α upregulated RSK4 expression when stably transfected into ECA109 and EC9706 cells, while knockdown of ΔNp63 decreased the level of RSK4 in TE10 and TE11 cells **(Figure 4G and 4H)**. By contrast, the RSK2 protein levels and phosphorylation of its known downstream substrates HSP27 and CREB, which have been implicated in SCC (12), were not significantly affected by ΔNp63 overexpression or downregulation **(Supplementary Figure 3K)**. Therefore, it appears that ΔNp63α transcriptionally regulates RSK4 expression but not RSK2 expression in ESCC. From transcription factor prediction analysis, a putative p63 binding site between -644 and -625 upstream of the transcriptional initiation site in the *RPS6KA6* promoter was identified **(Figure**

4A). Luciferase reporter assays showed that the *RPS6KA6* promoter activity was greatly enhanced in HEK293T cells transfected with ΔNp63α, whereas a deletion mutation of this p63 binding site nullified this transactivation **(Figure 4I)**. Exogenous and endogenous chromatin immunoprecipitation assays confirmed the direct binding of ΔNp63α to the *RPS6KA6* promoter in both ECA109 cells and TE10 cells **(Figure 4J and Supplementary Figure 3L)**. Taken together, these results suggest that RSK4 is highly upregulated together with ΔNp63 in ESCC and that *RPS6KA6* is a ΔNp63α target gene.

RSK4 mediates the ΔNp63α-enhanced CSC properties and radioresistance of ESCC cells

To investigate the involvement of RSK4 in the function of ΔNp63α in ESCC, we generated an ECA109 clone with ΔNp63α overexpression and RSK4 knockdown and a TE10 clone with ΔNp63 knockdown and RSK4 overexpression **(Supplementary Figure 4A)**. ΔNp63α overexpression led ECA109 cells to acquire CSC properties as evidenced by the increased sphere formation ability, ALDH activity, percentage of $CD90^+$ cells and protein levels of CD271, ABCG2, BMI-1, NANOG, OCT4 and SOX2. However, the ΔNp63α-induced CSC properties were largely abolished by RSK4 knockdown. Similar results were also obtained in TE10 cells, in which the reduction in CSC properties through ΔNp63 knockdown was partially rescued by RSK4 overexpression **(Figure 5A-5C and Supplementary Figure 4B)**. With respect to radioresistance, ESCC cells with ΔNp63α overexpression had a significantly increased

colony forming ability and decreased caspase-3 activity after irradiation, whereas ΔNp63α-induced radioresistance was largely impaired by RSK4 knockdown. By contrast, RSK4 overexpression greatly restored the radioresistance of ΔNp63 knockdown cells **(Figure 5D and 5E)**. The activating phosphorylation of checkpoint proteins ATM and CHK2 induced by irradiation was significantly increased in ΔNp63α-overexpressing ECA109 cells, whereas ΔNp63α-induced DNA damage checkpoint responses were largely impaired by RSK4 knockdown. Similar results were also obtained in TE10 cells, in which the inhibition of DNA damage checkpoint responses through ΔNp63 knockdown was partially rescued by RSK4 overexpression **(Figure 5F)**. The comet assay showed that ESCC cells with ΔNp63α overexpression had a significantly increased DNA damage repair efficiency; however, the ΔNp63α-induced DNA repair efficiency was largely abolished by RSK4 knockdown. By contrast, RSK4 overexpression greatly restored the DNA repair efficiency of ΔNp63 knockdown cells **(Supplementary Figure 4C)**. This result was further confirmed by assessing the dynamic changes in γ-H2AX levels after irradiation **(Figure 5G)**. Altogether, these results suggest that RSK4 is essential for ΔNp63α-mediated CSC properties and the radioresistance of ESCC cells.

RSK4 directly phosphorylates GSK-3β Ser9 in ESCC

To further investigate the mechanism underlying the role of RSK4 in ESCC, we performed a MAPK pathway phosphor-antibody array analysis **(Supplementary Table 4)** of ESCC cell lines with exogenous RSK4 expression after treatment with the RSK

inhibitor BI-D1870. With respect to the identified phosphorylated proteins, we found GSK-3β, a major serine/threonine kinase that is aberrantly activated in various cancer types and is involved in CSC properties and therapy resistance (38), to be highly phosphorylated at serine residue 9 (Ser9) in ECA109 cells expressing RSK4, while treatment with the RSK inhibitor BI-D1870 decreased the level of GSK-3β Ser9 phosphorylation **(Figure 6A)**. Moreover, Western blotting showed that RSK4 knockdown reduced the ΔNp63α-induced phosphorylation of GSK-3β Ser9, whereas the reduction in phosphorylated GSK-3β Ser9 through ΔNp63 knockdown was rescued by RSK4 overexpression **(Figure 6B)**. Sequence alignment analysis showed that Ser9 of GSK-3β is highly conserved from fruit fly to human, suggesting that this phosphorylation site may have important biological functions **(Supplementary Figure 5A).** Based on these results, we propose that RSK4 may directly phosphorylate GSK-3β Ser9. The results of an in vitro kinase assay showed that active RSK4 protein directly phosphorylated GSK-3β Ser9, with phosphorylation of RPS6 at Ser235/236 used as a positive control **(Figure 6C)**. The phosphorylation level of GSK-3β was inhibited in vitro when treated with BI-D1870 **(Supplementary Figure 5B)**, which was confirmed using an antibody that specifically detects GSK-3β phosphor-Ser9 **(Figure 6D)**. Moreover, RSK4 and GSK-3β colocalized in ESCC cells **(Supplementary Figure 5C)**, and the results of glutathione S-transferase (GST) pulldown assays as well as exogenous and endogenous co-immunoprecipitation assays confirmed the direct binding of RSK4 to GSK-3β **(Figure 6E, 6F and Supplementary Figure 5D)**. Molecular mapping using truncated RSK4 revealed that the N-terminal kinase domain

(NTKD) was responsible for the interaction with GSK-3β **(Figure 6G)**.

The correlation between RSK4 and phosphorylated GSK-3β Ser9 was also found in ESCC samples by IHC **(Supplementary Figure 5E)**. Clinical association studies found that upregulation of the phosphorylated GSK-3β Ser9 protein was associated with lymph node metastasis and vascular invasion **(Supplementary Table 5)**, similar to RSK4. Kaplan-Meier survival analysis showed that ESCC patients with higher phosphorylated GSK-3β Ser9 protein levels had worse OS and PFS than their low expression counterparts **(Supplementary Figure 5F)**. In summary, RSK4 phosphorylates GSK-3β Ser9 through direct interactions in ESCC cells, and coexpression of RSK4 and p-GSK-3β has prognostic value for clinical ESCC.

RSK4 stabilizes β-catenin through phosphorylating GSK-3β Ser9 in ESCC cells

It has been reported that the Wnt/β-catenin signaling pathway is closely involved in the maintenance and associated radioresistance of CSCs (39). The protein expression and nuclear localization of β-catenin are tightly regulated by GSK-3β, with phosphorylation of GSK-3β at Ser9 leading to reduced degradation of β-catenin, followed by its subsequent nuclear translocation (40). Here, we examined whether this pathway is altered in response to the modulation of RSK4 in ESCC cells. Western blotting showed that a higher RSK4 level in ESCC cells was associated with a longer half-life and reduced ubiquitination of β-catenin **(Figure 7A and 7B)**. By contrast, RSK4 depletion or treatment with BI-D1870 accelerated β-catenin degradation, which was reversed by the addition of MG132, a proteasome inhibitor **(Figure 7C)**. Moreover,

RSK4 stabilized β-catenin in the presence of GSK-3β WT but not GSK-3β S9A in ESCC cells, which was similar to overexpression of GSK3β S9D (constitutively inactivated mutation) or adding the GSK3β inhibitor AR-A014418 **(Figure 7D and 7E)**, further highlighting the importance of GSK-3β Ser9 phosphorylation by RSK4 for β-catenin stabilization. In addition, RSK4 promoted CSC properties and radioresistance in the presence of GSK-3β WT but not GSK-3β S9A in ESCC cells **(Figure 7F and 7G)**.

ΔNp63α overexpression dramatically increased the ratio of the nuclear β-catenin and β-catenin protein levels in both the cytoplasm and nucleus, whereas the increase was largely abolished by RSK4 knockdown in ECA109 cells. By contrast, TE10 cells with ΔNp63 downregulation exhibited significant restoration of β-catenin activity when RSK4 was overexpressed **(Figure 7H and Supplementary Figure 5G)**. The importance of these effects was strengthened by the assessment of the total and phosphorylated (inactive state) protein levels of β-catenin and expression of the Wnt/β-catenin pathway downstream targets MYC, CD44 and TCF1 **(Figure 7I)**. In addition, the *RPS6KA6* mRNA level was positively correlated with *HNF1A* (encoding TCF1) and *CD44* in ESCC specimens from the GEO cohorts **(Supplementary Figure 5H)**. To demonstrate that RSK4-dependent ESCC CSC properties and radioresistance are mediated through Wnt/β-catenin signaling, we treated RSK4-overexpressing ECA109 cells with the Wnt/β-catenin inhibitor iCRT3. Notably, inhibition of Wnt/β-catenin signaling greatly reduced the sphere formation ability of CSCs and increased caspase-3 activity after irradiation in RSK4-overexpressing cells **(Figure 7J, 7K and**

Supplementary Figure 5I), showing that this pathway mediates the upregulation of RSK4-dependent CSC properties and radioresistance in ESCC cells. Altogether, these results indicate that RSK4 phosphorylation of GSK-3β Ser9 is essential for activating the Wnt/β-catenin pathway to promote ESCC CSC properties and radioresistance.

Disrupting the RSK4 pathway reduces the CSC properties and improves the radiosensitivity of ESCC

Based on a computational simulation, we constructed a model of the three-dimensional structure of RSK4 NTKD by homology modeling and in silico docked BI-D1870, a highly specific and potent inhibitor of the NTKD of RSKs (41), to the ATP-binding site of RSK4. BI-D1870 had strong intermolecular interactions with the NTKD of RSK4 by forming two hydrogen bonds with the hinge region and another two hydrogen bonds with residues Lys105 and Asp216 **(Supplementary Figure 6A)**. BI-D1870 inhibited GSK-3β Ser9 phosphorylation in ESCC cells in a dose-dependent manner, with nearly 100% inhibition at a concentration of 10 μM **(Supplementary Figure 6B)**. At this concentration, BI-D1870 greatly suppressed CSC properties as well as β-catenin activity and expression of the Wnt/β-catenin pathway downstream targets of ESCC cells. However, RSK4 knockdown cells were not sensitive to BI-D1870 treatment compared with control cells, indicating that RSK4 is a key target of BI-D1870 for the inhibition of CSC properties and the Wnt/β-catenin pathway in ESCC cells **(Figure 8A-8D and Supplementary Figure 6C-6F)**. Furthermore, BI-D1870 inhibited ESCC CSC growth but had little effect on matched non-stem ESCC cells **(Supplementary Figure**

6G), indicating that BI-D1870 specifically disrupted ESCC CSC growth and maintenance. On the other hand, treatment of ESCC cells with BI-D1870, with RSK4 knockdown, or with both did not significantly change the expression levels of RSK1-3 proteins and the phosphorylation of their downstream substrates, indicating that RSK1-3 may not be involved with BI-D1870 to inhibit the malignant phenotypes of ESCC **(Supplementary Figure 6H)**.

We next examined whether RSK4 inhibition by BI-D1870 could improve the therapeutic efficacy of radiotherapy for treating ESCC. BI-D1870 or irradiation treatment each suppressed ESCC cell proliferation, while the combined treatment achieved the strongest proliferation inhibition **(Figure 8E)**. BI-D1870 or irradiation treatment each induced cell apoptosis, and the combined treatment again exhibited the strongest effect **(Figure 8F and Supplementary Figure 6I)**. These observations were supported by an assessment of the protein levels of the apoptosis markers cleaved caspase-3 and cleaved PARP **(Supplementary Figure 6J)**. Furthermore, the activating phosphorylation of checkpoint proteins ATM and CHK2 induced by irradiation was significantly decreased with BI-D1870 treatment **(Figure 8G)**, demonstrating that disrupting the RSK4 pathway reduced checkpoint activation in response to DNA damage. In addition, as assessed by immunofluorescent staining for γ-H2AX, combined treatment with BI-D1870 and irradiation induced more DNA damage than treatment with irradiation alone **(Figure 8H)**. This result was further confirmed by the comet assay after irradiation **(Supplementary Figure 6K)**, indicating that DNA damage repair was impaired by disrupting the RSK4 pathway. Concomitant treatment of tumor-

bearing mice with BI-D1870 and irradiation also reduced the growth and weight of ESCC xenograft tumors more significantly than treatment with each alone **(Figure 8I)**. Altogether, these results indicate that disruption of the RSK4 pathway by BI-D1870 suppresses the CSC properties and enhances the radiosensitivity of ESCC cells.

It has been reported that BI-D1870 has other targets such as PLK1 and Aurora B, whose IC50 values are 7-fold and 23-fold higher than that of RSK4 in vitro, respectively (41). To verify whether BI-D1870 had an off-target effect on PLK1 and Aurora B in ESCC cells, we performed a dose-response analysis to determine the BI-D1870 concentration that does not inhibit PLK1 and Aurora B in TE10 cells. We found that the expression levels of PLK1 and Aurora B proteins and the phosphorylation of their downstream substrates were not affected with the concentration of BI-D1870 at 5 μM **(Supplementary Figure 6L)**. At this concentration, GSK-3β Ser9 phosphorylation is strongly inhibited in TE10 cells **(Supplementary Figure 6B)**. Next, we tested whether BI-D1870 enhanced the radiosensitivity of ESCC cells at the concentration of 5 μM. Combined treatment of BI-D1870 and irradiation achieved the strongest proliferation inhibition and highest caspase-3 activity compared with each treatment alone **(Supplementary Figure 6M and 6N).** Moreover, combined treatment with BI-D1870 and irradiation induced more DNA content in the comet tail and higher γ-H2AX levels 6 h after irradiation than treatment with irradiation alone **(Supplementary Figure 6O and 6P)**. These results suggest that BI-D1870 can improve the radiosensitivity of ESCC cells at a concentration that does not inhibit PLK1 and Aurora B activity.

RSK4 inhibition with BI-D1870 sensitizes radiotherapy in ESCC patient-derived xenografts

Patient-derived xenograft (PDX) tumors are known to closely resemble primary tumors, and their use has transformed anticancer drug research, enabling the study of therapeutic responses and accelerating the transition from the bench to the clinic (42). We obtained ESCC tumors from 28 patients to establish PDX models, and nearly 80% of cases expressed the RSK4 protein at a high level, indicating that RSK4 overexpression is a common event in ESCC. However, there were no significant differences in RSK4 expression between PDX successful models and unsuccessful models **(Supplementary Figure 7A)**. Two PDX tumors (cases #03 and #06) with high RSK4 expression and one PDX tumor (cases #02) with negative RSK4 expression were selected for further analysis by IHC staining of grafted tumors collected from the animals. These tumors were all RSK2 protein-negative **(Supplementary Figure 7B)**. BI-D1870 strongly attenuated the growth and weight of high RSK4-expressing PDX tumors; in sharp contrast, BI-D1870 failed to reduce the growth and weight of RSK4-negative PDX tumors **(Figure 9A and Supplementary Figure 7C)**. The levels of Wnt/β-catenin pathway-associated and CSC-associated proteins and the Ki-67 index were greatly reduced, while apoptosis and DNA damage were significantly increased in RSK4-high, but not RSK4-negative, PDX tumors after BI-D1870 treatment **(Figure 9B-9D)**. Moreover, the growth curves of body weight; the histology of the liver, lung and kidney; and the results of functional tests of the liver and kidney from mice treated with BI-D1870 or the vehicle suggest that BI-D1870 is a well-tolerated agent without

severe toxicity to these organs **(Supplementary Figure 7D-7F)**. Finally, the combination of BI-D1870 and irradiation was even more effective at reducing tumor growth and weight in ESCC PDX models than treatment with each alone **(Figure 10A)**. Furthermore, IHC staining of cleaved caspase-3 and Ki-67 demonstrated that whereas BI-D1870 or irradiation treatment alone induced apoptosis and reduced proliferation of tumor cells in ESCC PDX models, the combined treatment resulted in much more apoptosis and greater proliferation inhibition **(Figure 10B)**. Taken together, these results verify that BI-D1870 inhibits tumor growth and improves the therapeutic efficacy of radiotherapy in ESCC PDX models and that the RSK4 expression level positively correlates with the therapeutic response.

Discussion

Here, we revealed RSK4 to be an oncogenic driver in ESCC that promotes CSC properties and radioresistance. RSK4 was first systematically identified as a direct target of ΔNp63α that is frequently amplified in ESCC. RSK4 phosphorylates GSK-3β at Ser9, activating the Wnt/β-catenin pathway, enhancing CSC properties, and increasing ESCC resistance to radiotherapy. Most importantly, pharmacologic inhibition of RSK4 using BI-D1870 markedly attenuates CSC properties and enhances the antitumor activity of radiotherapy in both nude mice and PDX models.

Our findings provide further evidence of the role of p63 as a key regulator in ESCC. ΔNp63α is the predominant p63 isoform expressed in basal epithelial cells and is

essential for squamous epithelial development (43). Furthermore, ΔNp63α is frequently overexpressed in ESCC and has been implicated in CSC properties (44, 45). Meera et al reported that ΔNp63α is associated with the B56α regulatory subunit of protein phosphatase 2A (PP2A), leading to inhibition of PP2A-mediated GSK-3β reactivation, which induces nuclear accumulation of β-catenin and activates β-catenin-dependent transcription in SCC (46). PP2A is a phosphatase that can mediate GSK-3β dephosphorylation, thereby increasing its activity (47). However, how ΔNp63α inhibits the activity of PP2A is not clear. Herein, we identified the functional link between p63 and the new target gene RSK4 and demonstrated the transcriptional regulation of RSK4 by ΔNp63α to activate the Wnt/β-catenin signaling pathway in ESCC, which could be another potential mechanism for ΔNp63α to promote CSC properties and radioresistance.

RSK4 has previously been reported to play different roles in multiple cancers. Dewdney et al reported that RSK4 is frequently hypermethylated in endometrial cancer compared with normal endometrial tissues (17). It was also found that RSK4 expression limits the oncogenic, invasive, and metastatic potential of breast cancer cells (18). These findings suggest that RSK4 may have an antitumor effect, which is further supported by the downregulation of RSK4 expression in ovarian cancer (19) and acute myeloid leukemia (20). By contrast, Thakur et al (25) observed that the expression of RSK4 mRNA was higher in transgenic mouse mammary tumors and human breast cancer tissues than in normal mammary tissues. Furthermore, RSK4 overexpression is associated with sunitinib resistance in kidney carcinoma and melanoma cell lines (21)

and can mediate resistance to PI3K pathway inhibitors in breast cancer (22), indicating that RSK4 may regulate treatment resistance and can promote tumor progression. Our laboratory has previously discovered that RSK4 is overexpressed in RCC as well as promotes cell cycle progression and enhances the invasive and metastatic capability of RCC cell lines (23). This study advanced our knowledge of the association of RSK4 in ESCC. Our data not only reveal roles for RSK4 in promoting ESCC CSC properties and radioresistance but also suggest RSK4 as a potential target for treating ESCC through pharmacologic inhibition. We have previously reported that the RSK4 protein may exist as several isoforms besides the known 84-kD form using a panel of antibodies (24). Distinct RSK4 isoforms may explain, to some extent, why RSK4 acts so differently in multiple cancers, as different isoforms may have unique or even opposite functions, such as the roles of STAT3 α and β in ESCC (48). In the present study, we used an antibody developed by The Human Protein Atlas project to study the role of RSK4 in ESCC, which makes our study more meaningful and consistent.

With regard to other members of the RSK family, RSK2 was reported to be involved in SCC progression (12). In the present study, no significant difference in RSK2 mRNA levels between ESCC and adjacent non-tumor tissues was found. Moreover, the protein levels of RSK2 and phosphorylation of its downstream targets were not significantly affected by ΔNp63 overexpression or downregulation in ESCC cells. In addition, RNA sequencing data generated under conditions of p63 depletion in human keratinocytes and SCC cell lines showed that only RSK4, rather than the other members of the RSK family, is downregulated by p63 knockdown. Furthermore, ESCC cells treated with BI-

D1870 did not evidently have altered levels of the RSK1-3 protein or phosphorylation of their downstream substrates. Altogether, these findings suggest that RSK4, but not other RSK family members, plays a key role in ESCC CSC properties and radioresistance.

Canonical Wnt/β-catenin signaling supports the formation and maintenance of CSCs and radioresistance (39). Consistent with the physiological roles of GSK-3β in negatively regulating canonical Wnt/β-catenin signaling, inhibition of GSK-3β is a prerequisite for the maintenance of CSC properties and radioresistance (40). Although it has been reported that RSK2 can phosphorylate GSK-3β at Ser9 (49), we found that GSK-3β was a binding partner and substrate of RSK4. To date, GSK-3β is the first direct substrate of RSK4 to be identified with direct evidence. RSK4 phosphorylated GSK-3β at Ser9 and reduced its activity, resulting in the enhancement of ESCC CSC properties and radioresistance by stabilizing β-catenin. Surprisingly, using an in vitro kinase assay, we also discovered that GSK-3β may directly phosphorylate RSK4 in turn **(Figure 5C)**. It is well known that a number of proteins phosphorylated by GSK-3β are targeted by E3-ubiquitin ligases, leading to subsequent proteasomal degradation, such as β-catenin (50), Snail (51) and Mcl-1 (52). Therefore, we speculate that RSK4 phosphorylated by GSK-3β may also be degraded in a proteasome-dependent manner, thus leading to more stabilized RSK4 when GSK-3β is inactivated by RSK4 phosphorylation, which is likely a previously unknown RSK4-GSK-3β feedback loop in ESCC.

Radiotherapy is a primary treatment option for locally advanced or unresectable

ESCC; however, there have been no significant improvements in OS of patients with advanced ESCC (53). The current concept to account for the increased mortality and therapy failure is that CSCs are mainly responsible for radioresistance and are the principal cause of cancer relapse (6, 54), suggesting that elimination of CSCs is crucial for improving ESCC treatment and overcoming its therapeutic resistance. However, CSC-targeting drugs are still unavailable in ESCC clinical practice. Thus, the development of anti-CSC therapeutics based on ESCC CSC-specific targets is promising for curing this type of cancer. In the search for CSC-specific functional targets in ESCC, we identified RSK4 as a molecular target and therapeutic candidate for the first time, as evidenced by its strong sphere forming ability and in vivo tumor initiating potential. These results are in line with evidence that RSK4 is constitutively activated under serum-starved conditions (16), which partly contributes to tumor sphere formation for acquiring stemness under serum-free conditions. There are several potential advantages of targeting RSK4 therapeutically: first, the preferential RSK4 upregulation in ESCC cells compared with the normal esophageal epithelium suggests a favorable therapeutic index for RSK4 inhibition in ESCC; second, RSK4 is critical for ESCC CSC proliferation and maintaining CSC self-renewal and tumorigenic potential, and thus, its pharmacological disruption would eradicate CSCs; third, inhibition of RSK4 significantly disrupts DNA damage checkpoint responses and DNA damage repair and increases the radiosensitivity of ESCC cells, suggesting a synergistic potential of RSK4 inhibition with radiotherapy in ESCC; and fourth, RSK4 is a kinase with ATP binding sites in its kinase domain, which makes it amenable for the

development of irreversible and specific small-molecule inhibitors (9). Our current study demonstrates that the combination of BI-D1870 and irradiation markedly attenuates tumor growth in ESCC xenografts and PDX models, suggesting that combinatorial RSK4 targeted therapy may enhance the efficacy of radiotherapy in ESCC.

Several small-molecule inhibitors have been reported that specifically target the NTKD or CTKD of RSKs. However, current RSK inhibitors target more than only one RSK isoform, which may limit their efficacy as therapeutic agents (55). BI-D1870 is a dihydropteridinone that reversibly binds the ATP pocket of the NTKD and is a more potent inhibitor of RSK4 than other RSK family members due to its lower IC_{50} for RSK4 than other RSKs (41). However, the disadvantages of BI-D1870 include its poor pharmacokinetic profile due to its poor stability, high clearance, and short plasma half-life (56, 57). It is suggested that the structural divergence between the NTKDs of the RSK isoforms could be exploited for the design of isoform-selective RSK inhibitors (55). Considering that RSK4 plays a significant role in ESCC progression, high-efficiency and specific RSK4 isoform-selective inhibitors urgently need to be developed in the future.

In conclusion, we established RSK4 as a key oncogenic factor in ESCC **(Supplementary Figure 8)**. This study not only describes a ΔNp63α-RSK4-GSK-3β axis to promote CSC properties and radioresistance in ESCC, but also reveals a clinical opportunity involving combined RSK4 inhibitor and radiotherapy for treating patients with ESCC. These findings establish a working model encompassing the function of

RSK4 acting on malignant progression and prognostic prediction in ESCC and reveal a promising drug target for treatment of these aggressive malignancies.

Methods

Cell culture, reagents and irradiation. HEK293T cells and human ESCC cell lines ECA109, EC9706, TE10 and TE11 were obtained from the Type Culture Collection of the Chinese Academy of Sciences (Shanghai, China). All cell lines were verified through short tandem repeat DNA profiling. Mycoplasma contamination was checked, and the test results were negative. Cells were cultured in DMEM (Thermo Fisher Scientific, Waltham, MA, USA) with 10% fetal bovine serum (Gibco, Carlsbad, CA, USA) at 37°C in an incubator with 5% CO_2. BI-D1870, AR-A014418, iCRT3 and MG-132 were purchased from Selleckchem, Inc. (Houston, TX, USA), and cycloheximide (CHX) was purchased from MCE (Monmouth Junction, NJ, USA). The cells and mice were irradiated by X-rays using the MBR-1520R-3 system (Hitachi Medico Technology, Tokyo, Japan) with the indicated dosages.

Tissue microarray. Multiple human normal and tumor organ tissue arrays were purchased from US Biomax Inc. (MC5003c, Rockville, MD, USA). This array contained 20 types of normal human tissues (5 cases for each type) and corresponding tumor tissues (20 cases for each type), including stomach, skin, prostate, brain, ovary, breast, testis, colon, bladder, uterus, thyroid, lung, head and neck, lymph node, soft tissue, liver, pancreas, kidney, cervix and esophagus **(Supplementary Table 1)**. ESCC

specimens and matched adjacent normal tissues were used to construct a tissue microarray (HEso-Squ180Sur-03, Shanghai Biochip Co., Ltd., Shanghai, China).

Immunohistochemistry. Paraffin-embedded tissues were sectioned at 4-μ m thickness. Slides were baked at 60 °C for 1 h and deparaffinized, rehydrated, and treated with 3% hydrogen peroxide for 10 min. Antigen retrieval was performed in citrate buffer, pH 6.0 in a steamer for 2 min or in Tris-EDTA buffer, pH 9.0 at 100°C for 20 min. After the slides were blocked with 5% BSA in PBS for 30 min, tissue sections were incubated overnight at 4°C with the indicated primary antibodies. Antibody information is shown in **Supplementary Table 6**. Subsequently, a standard rapid EnVision technique (Dako, Glostrup, Denmark) was utilized to detect the protein conjugates and develop the color. Finally, the sections were visualized after counterstaining with hematoxylin. Serial sections of ESCC were run in parallel with the primary antibody replaced by PBS and mouse IgG1 (Santa Cruz Biotechnology, CA, USA) as blank and negative controls.

Evaluation of immunohistochemical staining. The sections were photographed under an optical microscope (BX51, Olympus, Tokyo, Japan), and photos were captured by the software DP2-BSW (Olympus, Tokyo, Japan). Immunohistochemical staining was evaluated simultaneously by two observers who had no knowledge of clinicopathological features of the patients. The H-score is calculated by adding the multiplication of the different staining intensities in four gradations (0, 1+, 2+, 3+) with each percentage of positive cells. H-score = 1× (% cells 1+) + 2× (% cells 2+) + 3× (% cells 3+). Finally, a score from 0 to 300 points is obtained (58). We used the median H-score in the cohort as a cut-off to distinguish between high and low protein expression.

Clonogenic assay. Equal numbers of ESCC cells were plated in 6-cm tissue culture dishes at a clonogenic density (100 cells per dish) and allowed to adhere overnight. Subsequently, cells were irradiated with a single dose of 0, 3 or 6 Gy. Clonogenic assay procedures were performed as described previously (59). Survival fraction was calculated as follows: $(\text{number of colonies/number of cells plated})_{\text{irradiated}}$ /$(\text{number of colonies/number of cells plated})_{\text{non-irradiated}}$.

In vitro kinase assay. RSK4 active kinase and 10× kinase buffer were purchased from Millipore Corp. (Billerica, MA, USA). His-GSK-3β WT protein was purchased from Sino Biological (10044-H07B, Beijing, China). GSK-3β S9 peptide was synthesized by GL Biochem (Shanghai, China), and RPS6 peptide was purchased from Abcam (ab204879, Cambridge, MA, USA). His-GSK-3β S9A protein was expressed in *E. coli* BL21 bacteria. Bacteria were grown at 37°C to an absorbance of 0.6–0.8 at 600 nm and induced with 1 mM isopropyl β-D-thiogalactopyranoside (IPTG) at 30°C for 4 h. All proteins were purified using nickel-nitrilotriacetic acid agarose (Qiagen, Inc., Valencia, CA, USA) overnight at 4°C and eluted with 200 mM imidazole. After protein quantitation, the samples were separated by 10% SDS polyacrylamide gel for electrophoresis (SDS-PAGE) and visualized by Coomassie Brilliant Blue staining. The GSK-3β WT and GSK-3β S9A substrate (1 μg) and the active kinase (0.2 μg) in a 30-μL reaction were incubated at 37°C for 40 min with 1× kinase buffer containing 100 μmol/L unlabeled ATP (9804, Cell Signaling Technology) or 1 μCi [γ-^{32}P] ATP (NEG502A, Thermo Fisher Scientific, Waltham, MA, USA). The samples were added to 5× SDS buffer and then resolved by SDS-PAGE and visualized by autoradiography

or Western blot. The input was confirmed using an identical experimental set with a silver stain kit (CW2012, CW Biotech).

Patient-derived xenograft (PDX) tumors and drug sensitivity assay. PDX tumors were generated as described previously (60). Fresh tumor specimens were procured from previously established PDX models (passage 2–3) and cut into small tissue blocks (~50 mm^3) before being engrafted subcutaneously into male BALB/c nude mice. Xenografts were allowed to grow until they reached a size of 100-200 mm^3, and then mice were randomized into two groups (6 animals per group) for treatment. BI-D1870 was administered at 50 mg/kg dissolved in DMSO and sterile saline by daily intraperitoneal injections for 28 consecutive days. Drug vehicle-treated mice received daily injections of identical solution without BI-D1870. Tumor size was measured every 3 days by a digital caliper using the following formula: length×$width^2$×0.5. Investigators were blinded to the case number and the correspondent RSK4 level during the experiment. At the end of treatment, all mice were euthanized, and tumors were excised and weighed. The lung, liver and kidney of mice were removed for pathological examination, and serological examination of alanine transaminase (ALT), aspartate amino transferase (AST), blood urea nitrogen (BUN) and creatinine (Cr) was performed with a Chemray 240 automatic biochemical analyzer (Rayto, Shenzhen, China). To evaluate changes in tumor volume after each therapeutic regimen in PDX models, when tumors had grown to a volume of 100-200 mm^3, mice were randomized into four groups (6 mice per group): Vehicle; Vehicle+IR (ionizing radiation); BI-D1870; and BI-D1870+IR. A total of 10 Gy (5 Gy×2 times) was delivered to animals restrained in

custom lead jigs for localized IR treatment at the 7^{th} and 14^{th} day after dividing groups. BI-D1870 was administered at 50 mg/kg via intraperitoneal injection daily. Animals were raised for 25 days, and tumor volume was measured every 5 days and calculated by length × $width^2$×0.5. All animals were housed in a virus-free facility and maintained in a temperature and light (12 h light/dark cycle) controlled animal facility.

Data mining. The ESCC cohort of The Cancer Genome Atlas (TCGA) database (https://portal.gdc.cancer.gov/) was utilized to analyze mRNA expression of RSK4 in ESCC and its association with clinical data and the CSC marker ALDH1. The Genotype-Tissue Expression (GTEx) database (https://www.gtexportal.org/) was used to detect the correlation between TP63 and RSK4 mRNA in esophageal mucosa. The JASPAR database (jaspar.genereg.net/) was used to predict potential transcription factor binding site on RSK4 promoter. The Gene Expression Omnibus (GEO) dataset (https://www.ncbi.nlm.nih.gov/geo/) (GSE 20347 (61)) was used to analyze the correlation between TP63 and RSK4 mRNA in ESCC. GEO datasets (GSE 3108 (62) and GSE 4975 (63)) were used to show the effect of p63 depletion on RSK4 mRNA expression. GEO datasets (GSE 23400 (64) and GSE 32701 (65)) were used to analyze the correlation between RSK4 mRNA and Wnt/β-catenin pathway targets TCF1 and CD44 in ESCC. The raw data were downloaded from these datasets and manually graphed in Prism 7.0 (GraphPad Software, La Jolla, CA) with relative mRNA alterations.

Statistics. Data are expressed as the means ± SD. Statistical analysis was carried out as described in each corresponding figure legend. Comparisons between two groups were

performed by unpaired or paired 2-tailed Student's t test, while the comparison for more than 2 groups was conducted using 1-way ANOVA with Tukey's post hoc test. Differences among variables were assessed by Chi-square test. The correlation between groups was determined by Pearson's correlation test. The survival rates were analyzed by the Kaplan-Meier method. Log-rank test was used to compare the survival of patients between subgroups. Multivariate analyses were performed by the multivariate Cox proportional hazard regression model. Sample number (n) indicates the number of independent biological samples in each experiment. Sample numbers and experimental repeats are indicated in figures and figure legends. Generally, all experiments were replicated at least three independent times. *P* value less than 0.05 was considered statistically significant. Analyses were performed using Prism 7.0 (GraphPad Software, La Jolla, CA).

Study approval. Ethical approval was obtained from Xijing Hospital Research Ethics Committee, and written informed consent was obtained from each patient. All experimental procedures were performed in accordance with relevant institutional and national guidelines and approved by the Institutional Animal Care and Use Committee of Fourth Military Medical University.

Author contributions

MYL designed and performed the experiments, analyzed data and wrote the manuscript; LNF and DHH performed animal experiments and analyzed data; ZY, JM, and YXL performed the bioinformatics analysis; PFL, DHZ, and JC performed Western blot

experiments and histopathological analysis; LJ and SLL performed homology modeling; JJX and QHD performed the in vitro kinase assay; JY, MS, YZN, KCW, DJL, YS, YW, QGY, SPG, and XWB wrote the manuscript and provided important advice for this study; FZ, JZ, and ZW designed experiments, wrote the manuscript and supervised the study. All authors read the manuscript and approved the study.

Acknowledgments

This work was supported by grants from the National Natural Science Foundation of China (81272651, 81570180, 81421003, 81770523 and 81472402) and the State Key Laboratory of Cancer Biology (CBSKL2014Z07). We thank Deng-Xu Tan (Laboratory Animal Center, Fourth Military Medical University) and for the assistance in establishing the PDX models. We thank Pei-Pei Xue and Ling Zou (Department of Biochemistry and Molecular Biology, Huazhong University of Science and Technology) for the help with in vitro kinase analyses. We thank Dr. Hui-Ping Liu (Department of Pharmacology, Feinberg School of Medicine, Northwestern University) for the important suggestions on this study.

References

1. Abnet CC, Arnold M, Wei WQ. Epidemiology of Esophageal Squamous Cell Carcinoma. *Gastroenterology.* 2018;154(2):360-373.
2. Chen W, et al. Cancer statistics in China, 2015. *CA Cancer J Clin.* 2016;66(2):115-132.
3. Liang H, Fan JH, Qiao YL. Epidemiology, etiology, and prevention of esophageal squamous cell carcinoma in China. *Cancer Biol Med.* 2017;14(1):33-41.
4. van Hagen P, et al. Preoperative chemoradiotherapy for esophageal or junctional cancer. *The New England journal of medicine.* 2012;366(22):2074-2084.
5. Plaks V, Kong N, Werb Z. The cancer stem cell niche: how essential is the niche in regulating stemness of tumor cells? *Cell Stem Cell.* 2015;16(3):225-238.
6. Wang D, Plukker JTM, Coppes RP. Cancer stem cells with increased metastatic potential as a

therapeutic target for esophageal cancer. *Seminars in cancer biology.* 2017;44:60-66.
7. Krause M, Dubrovska A, Linge A, Baumann M. Cancer stem cells: Radioresistance, prediction of radiotherapy outcome and specific targets for combined treatments. *Advanced drug delivery reviews.* 2017;109:63-73.
8. Chen GZ, et al. The mechanisms of radioresistance in esophageal squamous cell carcinoma and current strategies in radiosensitivity. *J Thorac Dis.* 2017;9(3):849-859.
9. Anjum R, Blenis J. The RSK family of kinases: emerging roles in cellular signalling. *Nat Rev Mol Cell Biol.* 2008;9(10):747-758.
10. Romeo Y, Zhang X, Roux PP. Regulation and function of the RSK family of protein kinases. *Biochem J.* 2012;441(2):553-569.
11. Zhou Y, et al. Crucial roles of RSK in cell motility by catalysing serine phosphorylation of EphA2. *Nat Commun.* 2015;6:7679.
12. Kang S, et al. p90 ribosomal S6 kinase 2 promotes invasion and metastasis of human head and neck squamous cell carcinoma cells. *J Clin Invest.* 2010;120(4):1165-1177.
13. Zhao H, et al. The Clinical Implications of RSK1-3 in Human Breast Cancer. *Anticancer Res.* 2016;36(3):1267-1274.
14. Bignone PA, et al. RPS6KA2, a putative tumour suppressor gene at 6q27 in sporadic epithelial ovarian cancer. *Oncogene.* 2007;26(5):683-700.
15. Yntema HG, et al. A novel ribosomal S6-kinase (RSK4; RPS6KA6) is commonly deleted in patients with complex X-linked mental retardation. *Genomics.* 1999;62(3):332-343.
16. Dummler BA, et al. Functional characterization of human RSK4, a new 90-kDa ribosomal S6 kinase, reveals constitutive activation in most cell types. *J Biol Chem.* 2005;280(14):13304-13314.
17. Dewdney SB, et al. Aberrant methylation of the X-linked ribosomal S6 kinase RPS6KA6 (RSK4) in endometrial cancers. *Clin Cancer Res.* 2011;17(8):2120-2129.
18. Thakur A, et al. Anti-invasive and antimetastatic activities of ribosomal protein S6 kinase 4 in breast cancer cells. *Clin Cancer Res.* 2008;14(14):4427-4436.
19. Arechavaleta-Velasco F, et al. Ribosomal S6 kinase 4 (RSK4) expression in ovarian tumors and its regulation by antineoplastic drugs in ovarian cancer cell lines. *Med Oncol.* 2016;33(2):11.
20. Rafiee M, et al. Down-Regulation of Ribosomal S6 kinase RPS6KA6 in Acute Myeloid Leukemia Patients. *Cell J.* 2016;18(2):159-164.
21. Bender C, Ullrich A. PRKX, TTBK2 and RSK4 expression causes Sunitinib resistance in kidney carcinoma- and melanoma-cell lines. *Int J Cancer.* 2012;131(2):E45-55.
22. Serra V, et al. RSK3/4 mediate resistance to PI3K pathway inhibitors in breast cancer. *J Clin Invest.* 2013;123(6):2551-2563.
23. Fan L, et al. Ribosomal s6 protein kinase 4: a prognostic factor for renal cell carcinoma. *Br J Cancer.* 2013;109(5):1137-1146.
24. Sun Y, et al. Basic anatomy and tumor biology of the RPS6KA6 gene that encodes the p90 ribosomal S6 kinase-4. *Oncogene.* 2013;32(14):1794-1810.
25. Thakur A, et al. Aberrant expression of X-linked genes RbAp46, Rsk4, and Cldn2 in breast cancer. *Mol Cancer Res.* 2007;5(2):171-181.
26. Cancer Genome Atlas Research N, et al. Integrated genomic characterization of oesophageal carcinoma. *Nature.* 2017;541(7636):169-175.
27. Su X, Chakravarti D, Flores ER. p63 steps into the limelight: crucial roles in the suppression of

tumorigenesis and metastasis. *Nat Rev Cancer.* 2013;13(2):136-143.
28. Sethi I, et al. A global analysis of the complex landscape of isoforms and regulatory networks of p63 in human cells and tissues. *BMC Genomics.* 2015;16:584.
29. Thepot A, et al. Intraepithelial p63-dependent expression of distinct components of cell adhesion complexes in normal esophageal mucosa and squamous cell carcinoma. *Int J Cancer.* 2010;127(9):2051-2062.
30. Saladi SV, et al. ACTL6A Is Co-Amplified with p63 in Squamous Cell Carcinoma to Drive YAP Activation, Regenerative Proliferation, and Poor Prognosis. *Cancer Cell.* 2017;31(1):35-49.
31. Yang L, et al. ALDH1A1 defines invasive cancer stem-like cells and predicts poor prognosis in patients with esophageal squamous cell carcinoma. *Mod Pathol.* 2014;27(5):775-783.
32. Kreso A, Dick JE. Evolution of the cancer stem cell model. *Cell Stem Cell.* 2014;14(3):275-291.
33. Hu Y, Smyth GK. ELDA: extreme limiting dilution analysis for comparing depleted and enriched populations in stem cell and other assays. *J Immunol Methods.* 2009;347(1-2):70-78.
34. Jackson SP, Bartek J. The DNA-damage response in human biology and disease. *Nature.* 2009;461(7267):1071-1078.
35. Lanz MC, Dibitetto D, Smolka MB. DNA damage kinase signaling: checkpoint and repair at 30 years. *The EMBO journal.* 2019;38(18):e101801.
36. Hibi K, et al. AIS overexpression in advanced esophageal cancer. *Clin Cancer Res.* 2001;7(3):469-472.
37. Lo Muzio L, et al. p63 overexpression associates with poor prognosis in head and neck squamous cell carcinoma. *Hum Pathol.* 2005;36(2):187-194.
38. Domoto T, et al. Glycogen synthase kinase-3beta is a pivotal mediator of cancer invasion and resistance to therapy. *Cancer Sci.* 2016;107(10):1363-1372.
39. Fodde R, Brabletz T. Wnt/beta-catenin signaling in cancer stemness and malignant behavior. *Curr Opin Cell Biol.* 2007;19(2):150-158.
40. Trowbridge JJ, Xenocostas A, Moon RT, Bhatia M. Glycogen synthase kinase-3 is an in vivo regulator of hematopoietic stem cell repopulation. *Nat Med.* 2006;12(1):89-98.
41. Sapkota GP, et al. BI-D1870 is a specific inhibitor of the p90 RSK (ribosomal S6 kinase) isoforms in vitro and in vivo. *Biochem J.* 2007;401(1):29-38.
42. Aparicio S, Hidalgo M, Kung AL. Examining the utility of patient-derived xenograft mouse models. *Nat Rev Cancer.* 2015;15(5):311-316.
43. Daniely Y, et al. Critical role of p63 in the development of a normal esophageal and tracheobronchial epithelium. *Am J Physiol Cell Physiol.* 2004;287(1):C171-181.
44. Melino G, Memmi EM, Pelicci PG, Bernassola F. Maintaining epithelial stemness with p63. *Sci Signal.* 2015;8(387):re9.
45. Nekulova M, Holcakova J, Coates P, Vojtesek B. The role of p63 in cancer, stem cells and cancer stem cells. *Cell Mol Biol Lett.* 2011;16(2):296-327.
46. Patturajan M, et al. DeltaNp63 induces beta-catenin nuclear accumulation and signaling. *Cancer Cell.* 2002;1(4):369-379.
47. Seeling JM, et al. Regulation of beta-catenin signaling by the B56 subunit of protein phosphatase 2A. *Science.* 1999;283(5410):2089-2091.
48. Zhang HF, et al. The Opposing Function of STAT3 as an Oncoprotein and Tumor Suppressor

Is Dictated by the Expression Status of STAT3beta in Esophageal Squamous Cell Carcinoma. *Clin Cancer Res.* 2016;22(3):691-703.

49. Lee CJ, et al. RSK2-induced stress tolerance enhances cell survival signals mediated by inhibition of GSK3beta activity. *Biochemical and biophysical research communications.* 2013;440(1):112-118.
50. Aberle H, Bauer A, Stappert J, Kispert A, Kemler R. beta-catenin is a target for the ubiquitin-proteasome pathway. *The EMBO journal.* 1997;16(13):3797-3804.
51. Zhou BP, et al. Dual regulation of Snail by GSK-3beta-mediated phosphorylation in control of epithelial-mesenchymal transition. *Nat Cell Biol.* 2004;6(10):931-940.
52. Ding Q, et al. Degradation of Mcl-1 by beta-TrCP mediates glycogen synthase kinase 3-induced tumor suppression and chemosensitization. *Mol Cell Biol.* 2007;27(11):4006-4017.
53. He L, et al. Re-evaluating the optimal radiation dose for definitive chemoradiotherapy for esophageal squamous cell carcinoma. *J Thorac Oncol.* 2014;9(9):1398-1405.
54. Islam F, Gopalan V, Wahab R, Smith RA, Lam AK. Cancer stem cells in oesophageal squamous cell carcinoma: Identification, prognostic and treatment perspectives. *Crit Rev Oncol Hematol.* 2015;96(1):9-19.
55. Casalvieri KA, Matheson CJ, Backos DS, Reigan P. Selective Targeting of RSK Isoforms in Cancer. *Trends Cancer.* 2017;3(4):302-312.
56. Pambid MR, et al. Overcoming resistance to Sonic Hedgehog inhibition by targeting p90 ribosomal S6 kinase in pediatric medulloblastoma. *Pediatr Blood Cancer.* 2014;61(1):107-115.
57. Hammoud L, et al. Identification of RSK and TTK as Modulators of Blood Vessel Morphogenesis Using an Embryonic Stem Cell-Based Vascular Differentiation Assay. *Stem Cell Reports.* 2016;7(4):787-801.
58. Specht E, et al. Comparison of immunoreactive score, HER2/neu score and H score for the immunohistochemical evaluation of somatostatin receptors in bronchopulmonary neuroendocrine neoplasms. *Histopathology.* 2015;67(3):368-377.
59. Frankle RT. Nutrition education in the medical school curriculum: a proposal for action: a curriculum design. *Am J Clin Nutr.* 1976;29(1):105-109.
60. Zhang Y, et al. PP2AC Level Determines Differential Programming of p38-TSC-mTOR Signaling and Therapeutic Response to p38-Targeted Therapy in Colorectal Cancer. *EBioMedicine.* 2015;2(12):1944-1956.
61. Hu N, et al. Genome wide analysis of DNA copy number neutral loss of heterozygosity (CNNLOH) and its relation to gene expression in esophageal squamous cell carcinoma. *BMC Genomics.* 2010;11:576.
62. Koster MI, Kim S, Huang J, Williams T, Roop DR. TAp63alpha induces AP-2gamma as an early event in epidermal morphogenesis. *Dev Biol.* 2006;289(1):253-261.
63. Barbieri CE, Tang LJ, Brown KA, Pietenpol JA. Loss of p63 leads to increased cell migration and up-regulation of genes involved in invasion and metastasis. *Cancer Res.* 2006;66(15):7589-7597.
64. Su H, et al. Global gene expression profiling and validation in esophageal squamous cell carcinoma and its association with clinical phenotypes. *Clin Cancer Res.* 2011;17(9):2955-2966.
65. Aoyagi K, et al. Artificially induced epithelial-mesenchymal transition in surgical subjects: its implications in clinical and basic cancer research. *PLoS One.* 2011;6(4):e18196.

Figure 1

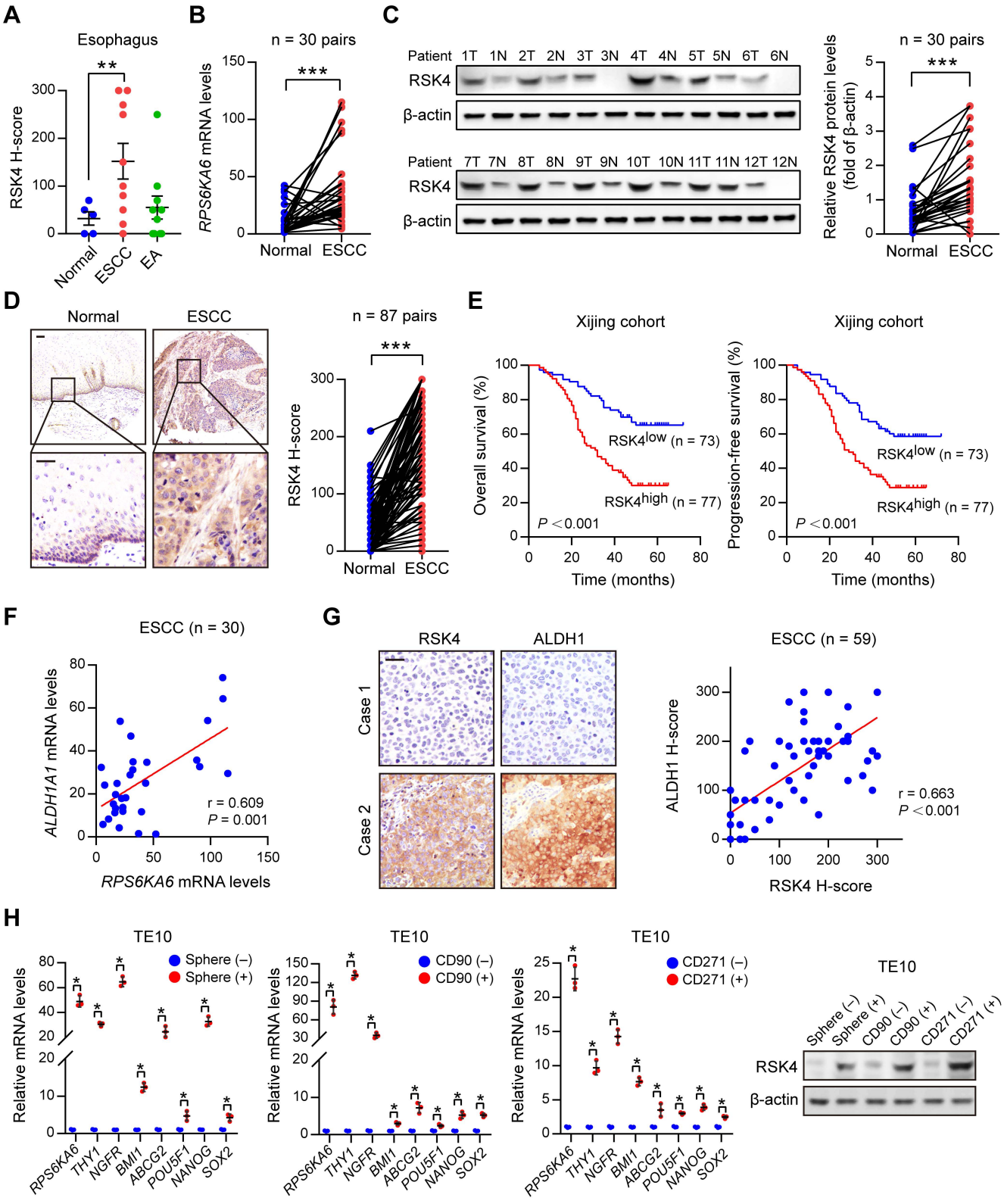
A
Esophagus
RSK4 H-score
Normal
ESCC
EA
B
n = 30 pairs
RPS6KA6 mRNA levels
Normal
ESCC
C
Patient 1T 1N 2T 2N 3T 3N 4T 4N 5T 5N 6T 6N
RSK4
β-actin
Patient 7T 7N 8T 8N 9T 9N 10T 10N 11T 11N 12T 12N
RSK4
β-actin
n = 30 pairs
Relative RSK4 protein levels (fold of β-actin)
Normal
ESCC
D
Normal
ESCC
n = 87 pairs
RSK4 H-score
Normal
ESCC
E
Xijing cohort
Overall survival (%)
RSK4low (n = 73)
RSK4high (n = 77)
P <0.001
Time (months)
Xijing cohort
Progression-free survival (%)
RSK4low (n = 73)
RSK4high (n = 77)
P <0.001
Time (months)
F
ESCC (n = 30)
ALDH1A1 mRNA levels
r = 0.609
P = 0.001
RPS6KA6 mRNA levels
G
RSK4
ALDH1
Case 1
Case 2
ESCC (n = 59)
ALDH1 H-score
r = 0.663
P <0.001
RSK4 H-score
H
TE10
Sphere (–)
Sphere (+)
Relative mRNA levels
RPS6KA6
THY1
NGFR
BMI1
ABCG2
POU5F1
NANOG
SOX2
TE10
CD90 (–)
CD90 (+)
TE10
CD271 (–)
CD271 (+)
TE10
Sphere (–)
Sphere (+)
CD90 (–)
CD90 (+)
CD271 (–)
CD271 (+)
RSK4
β-actin

Figure 1. RSK4 is highly expressed in ESCC CSCs. (A) RSK4 protein was highly expressed in ESCC rather than esophageal adenocarcinoma (EA) compared with corresponding non-tumor tissues. Representative immunohistochemical (IHC) staining images are shown in **Supplementary Figure 1A**. (B) mRNA levels of *RPS6KA6* in 30 pairs of ESCC samples and adjacent non-tumor tissues were determined by real-time PCR. *GAPDH* was used as a loading control. (C) Western blot analysis (left) and quantification of RSK4 expression (right) in ESCC tumor tissues (T) and adjacent non-tumor tissues (N) from 30 patients. The results of other samples are presented in **Supplementary Figure 1B**. Protein expression was normalized to β-actin levels. (D) Representative IHC staining images and H-score of RSK4 protein expression in ESCC tumor tissues and adjacent non-tumor tissues. Scale bars, 100 μm. (E) Kaplan-Meier estimation of ESCC overall survival (left) and progression-free survival (right) based on the RSK4 expression levels in the Xijing cohort. (F) Correlation between *RPS6KA6* and *ALDH1A1* mRNA expression in 30 ESCC patients. (G) Representative IHC staining images of RSK4 and ALDH1 protein expression in ESCC patients from the Xijing cohort. Scale bars, 100 μm. Correlation of IHC data of RSK4 and ALDH1 protein expression in 59 ESCC patients. (H) RSK4 was preferentially expressed in tumor spheres compared to non-spheres, and elevated RSK4 expression was detected in $CD90^+$ or $CD271^+$-enriched cell populations compared with the $CD90^-$ or $CD271^-$ cell subsets as assessed by real-time PCR (n = 3 independent experiments) and immunoblotting. Data are representative of means ± SD. $*P < 0.05$, $**P < 0.01$, $***P < 0.001$. Differences were tested using paired (B, C, D) and unpaired (H) 2-sided

Student’s t test, 1-way ANOVA with Tukey’s post hoc test (A) and Log-rank test (E). The correlation was determined by Pearson’s correlation test (F, G).

Figure 2

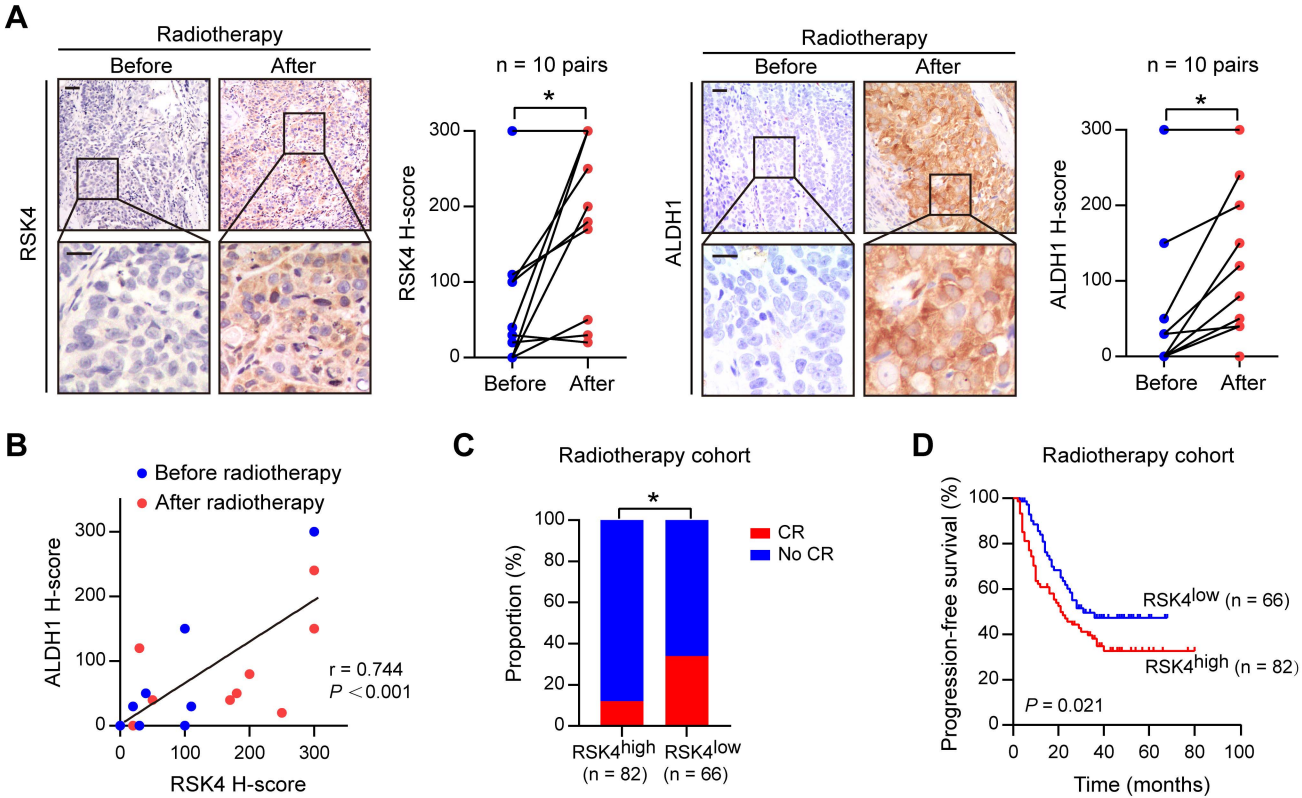
A
Radiotherapy
Before
After
RSK4
n = 10 pairs
RSK4 H-score
Before
After
ALDH1
ALDH1 H-score
B
Before radiotherapy
After radiotherapy
ALDH1 H-score
RSK4 H-score
r = 0.744
P < 0.001
C
Radiotherapy cohort
Proportion (%)
CR
No CR
RSK4high (n = 82)
RSK4low (n = 66)
D
Radiotherapy cohort
Progression-free survival (%)
RSK4low (n = 66)
RSK4high (n = 82)
P = 0.021
Time (months)

Figure 2. RSK4 is closely linked with the radioresistance and poor survival of ESCC patients. (A) Representative IHC staining images and IHC H-scores of RSK4 and ALDH1 protein expression in 10 ESCC patients before and after receiving radiotherapy. Scale bars, 100 μm. (B) The RSK4 protein levels were positively correlated with ALDH1 in these cases. (C) Radiotherapy ESCC patients with higher expression of RSK4 had a lower ratio of complete response (CR). (D) Kaplan–Meier estimation of the progression-free survival curves of 148 ESCC patients treated with radiotherapy according to the RSK4 expression levels in the primary tumor. *$P < 0.05$. Differences were tested using paired 2-sided Student's t test (A), Chi-square test (C) and Log-rank test (D). The correlation was determined by Pearson's correlation test (B).

Figure 3

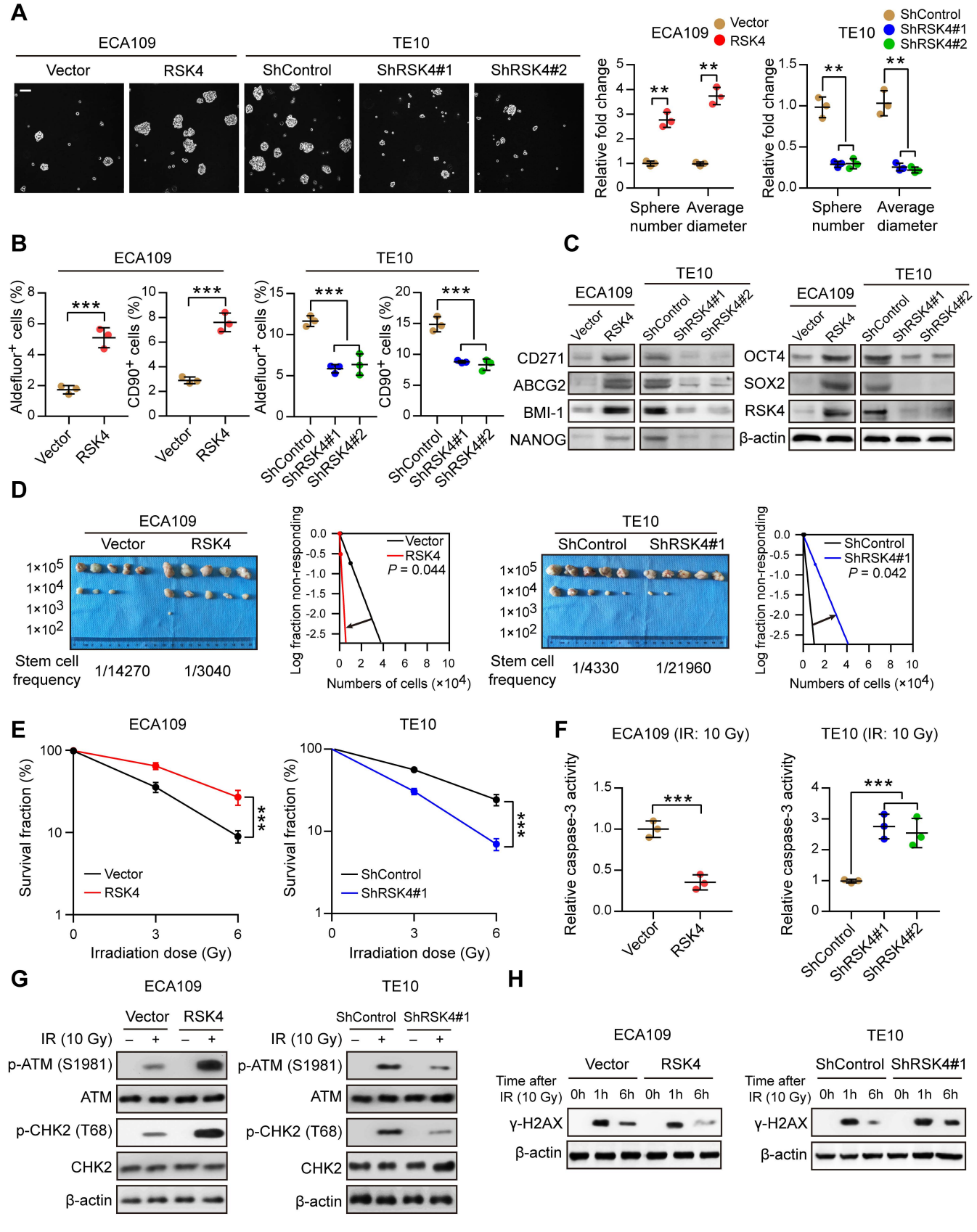
A
ECA109
TE10
Vector
RSK4
ShControl
ShRSK4#1
ShRSK4#2
Relative fold change
Sphere number
Average diameter
B
Aldefluor+ cells (%)
CD90+ cells (%)
C
CD271
ABCG2
BMI-1
NANOG
OCT4
SOX2
RSK4
β-actin
D
Stem cell frequency
1/14270
1/3040
1/4330
1/21960
Log fraction non-responding
Numbers of cells (×10^4)
P = 0.044
P = 0.042
E
Survival fraction (%)
Irradiation dose (Gy)
F
Relative caspase-3 activity
ECA109 (IR: 10 Gy)
TE10 (IR: 10 Gy)
G
IR (10 Gy)
p-ATM (S1981)
ATM
p-CHK2 (T68)
CHK2
β-actin
H
Time after IR (10 Gy)
0h 1h 6h 0h 1h 6h
γ-H2AX
β-actin

Figure 3. RSK4 promotes the CSC properties and radioresistance of ESCC cells. (A) Tumor sphere formation assay showing that RSK4 overexpression increased the sphere formation ability of ESCC cells, whereas RSK4 knockdown reduced their sphere formation ability (n = 3 independent experiments). Scale bars, 100 μm. (B) Flow cytometry analysis showing that RSK4-overexpressing cells had elevated ALDH activity and an increased proportion of $CD90^+$ cells, whereas RSK4-suppressed cells exhibited reduced ALDH activity and a reduced proportion of $CD90^+$ cells (n = 3 independent experiments). (C) Western blot analysis indicating that RSK4 overexpression increased ESCC CSC marker expression, whereas RSK4 knockdown had the opposite effect. (D) Limiting dilution analysis showing the higher tumorigenicity of RSK4-overexpressing ECA109 cells in NOD/SCID mice than control cells, but RSK4-knockdown TE10 cells had lower tumorigenicity than their control group (5 mice each). (E) Clonogenic survival assays of ESCC cells with overexpression or knockdown of RSK4 at the indicated irradiation doses (n = 3 independent experiments). (F) Relative caspase-3 activity 24 h after IR (10 Gy) of ESCC cells with overexpression or knockdown of RSK4 (n = 3 independent experiments). (G) Western blot analysis of phosphorylated and total amounts of checkpoint proteins ATM and CHK2 from the indicated groups before treatment (-) and 1h after 10 Gy of IR (+). (H) ESCC cells from the indicated groups were treated with IR (10 Gy) and recultured under normal conditions for 1 and 6 h, then subjected to Western blot analysis with γ-H2AX antibody. The "0 h" indicates cells with IR treatment but with no time for DNA repair. Data are representative of means ± SD. $^{**}P < 0.01$, $^{***}P < 0.001$. Differences

were tested using unpaired 2-sided Student’s t test (A, B, D, E, F).

Figure 4

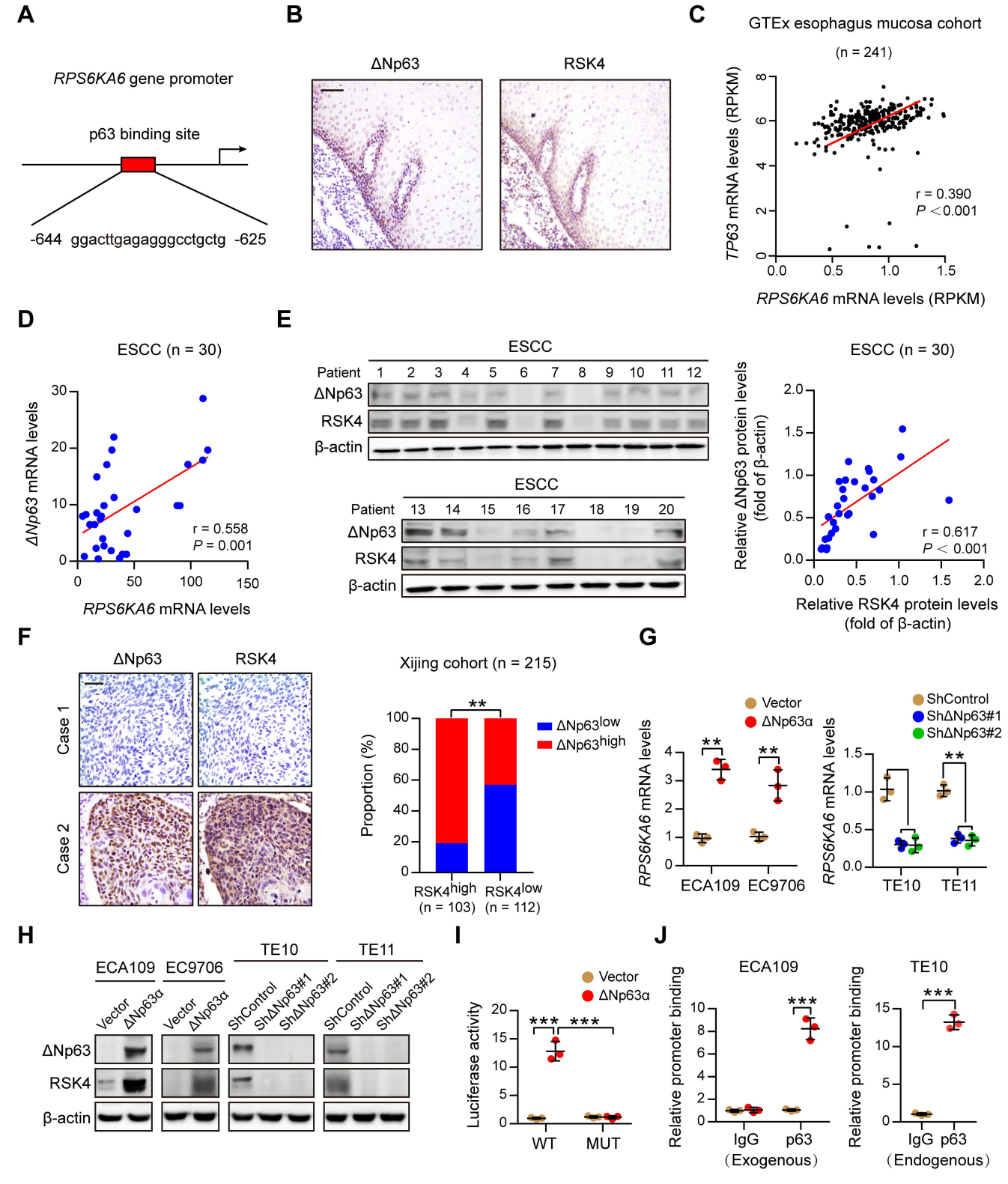
A
RPS6KA6 gene promoter
p63 binding site
-644 ggacttgagagggcctgctg -625
B
ΔNp63
RSK4
C
GTEx esophagus mucosa cohort
(n = 241)
TP63 mRNA levels (RPKM)
r = 0.390
P < 0.001
RPS6KA6 mRNA levels (RPKM)
D
ESCC (n = 30)
ΔNp63 mRNA levels
r = 0.558
P = 0.001
RPS6KA6 mRNA levels
E
ESCC
Patient 1 2 3 4 5 6 7 8 9 10 11 12
ΔNp63
RSK4
β-actin
ESCC
Patient 13 14 15 16 17 18 19 20
ΔNp63
RSK4
β-actin
ESCC (n = 30)
Relative ΔNp63 protein levels (fold of β-actin)
r = 0.617
P < 0.001
Relative RSK4 protein levels (fold of β-actin)
F
ΔNp63
RSK4
Case 1
Case 2
Xijing cohort (n = 215)
Proportion (%)
ΔNp63low
ΔNp63high
RSK4high (n = 103)
RSK4low (n = 112)
G
Vector
ΔNp63α
RPS6KA6 mRNA levels
ECA109
EC9706
ShControl
ShΔNp63#1
ShΔNp63#2
TE10
TE11
H
ECA109
EC9706
TE10
TE11
Vector
ΔNp63α
ShControl
ShΔNp63#1
ShΔNp63#2
ΔNp63
RSK4
β-actin
I
Vector
ΔNp63α
Luciferase activity
WT
MUT
J
ECA109
TE10
Relative promoter binding
IgG
p63
(Exogenous)
(Endogenous)

Figure 4. ΔNp63α directly transactivates RSK4 expression in ESCC. (A) Predicted binding sites for p63 in the promoter regions of *RPS6KA6*. (B) Immunohistochemical (IHC) analysis of the ΔNp63 and RSK4 proteins showing an identical coexpression pattern in serial sections of the esophageal epithelial basal and suprabasal layers. Scale bars, 50 μm. (C) Correlation between the *RPS6KA6* and *TP63* mRNA expression patterns in the Genotype-Tissue Expression (GTEx) esophagus mucosa dataset. (D) The mRNA levels of *ΔNp63* and *RPS6KA6* in 30 ESCC samples were determined by real-time PCR. *GAPDH* was used as a loading control. (E) Expression of ΔNp63 and RSK4 was detected by Western blot in 30 ESCC samples. The results of other samples are presented in **Supplementary Figure 3G.** Protein expression was normalized to the β-actin levels. (F) Representative IHC staining images of ΔNp63 and RSK4 protein expression in ESCC patients. Scale bars, 100 μm. Histograms showing the correlation of the IHC data for high or low RSK4 expression relative to the level of ΔNp63. (G) ΔNp63α overexpression upregulated whereas ΔNp63 silencing reduced *RPS6KA6* mRNA expression in ESCC cells (n = 3 independent experiments). (H) ΔNp63α overexpression upregulated whereas ΔNp63 silencing reduced RSK4 protein expression in ESCC cells. (I) ΔNp63α induced reporter activity of the wild-type (WT) *RPS6KA6* promoter rather than the p63 responsive element deletion mutant (MUT) promoter, as determined by a luciferase reporter assay in HEK293T cells (n = 3 independent experiments). (J) Exogenous (left) and endogenous (right) chromatin immunoprecipitation analysis of the interaction between the ΔNp63 and *RPS6KA6* promoter in ESCC cells (n = 3 independent experiments). Data are representative of

means ± SD. $^{**}P < 0.01$, $^{***}P < 0.001$. Differences were tested using unpaired 2-sided Student's t test (G, I, J) and Chi-square test (F). The correlation was determined by Pearson's correlation test (C, D, E).

Figure 5

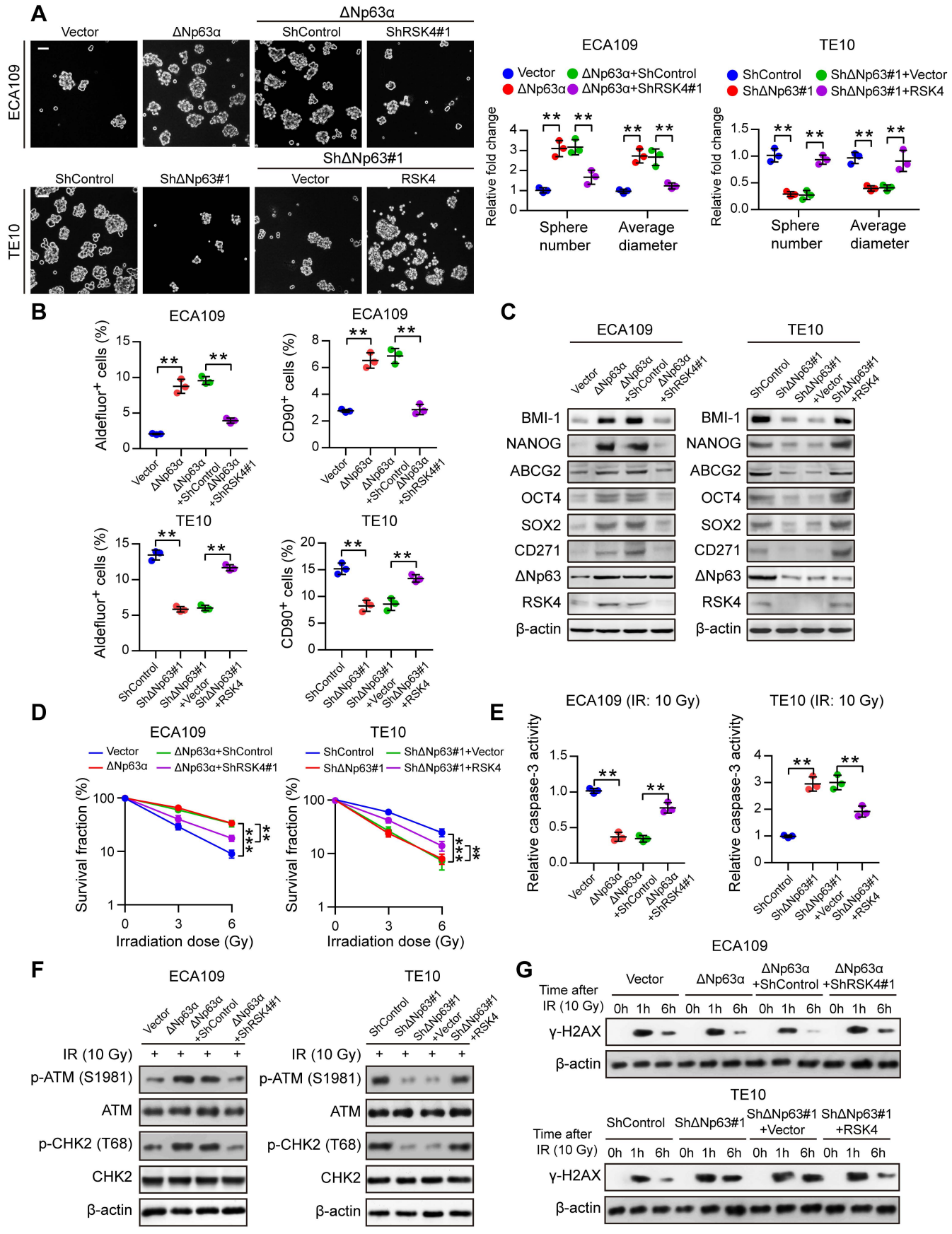
A
ΔNp63α
Vector
ΔNp63α
ShControl
ShRSK4#1
ECA109
ShΔNp63#1
ShControl
ShΔNp63#1
Vector
RSK4
TE10
ECA109
Vector
ΔNp63α
ΔNp63α+ShControl
ΔNp63α+ShRSK4#1
Relative fold change
Sphere number
Average diameter
TE10
ShControl
ShΔNp63#1
ShΔNp63#1+Vector
ShΔNp63#1+RSK4
B
ECA109
Aldefluor+ cells (%)
CD90+ cells (%)
TE10
C
ECA109
TE10
BMI-1
NANOG
ABCG2
OCT4
SOX2
CD271
ΔNp63
RSK4
β-actin
D
ECA109
TE10
Survival fraction (%)
Irradiation dose (Gy)
E
ECA109 (IR: 10 Gy)
TE10 (IR: 10 Gy)
Relative caspase-3 activity
F
ECA109
TE10
IR (10 Gy)
p-ATM (S1981)
ATM
p-CHK2 (T68)
CHK2
β-actin
G
ECA109
TE10
Time after IR (10 Gy)
0h 1h 6h
γ-H2AX
β-actin

Figure 5. RSK4 is essential for the ΔNp63α-mediated CSC properties and radioresistance of ESCC cells. (A) Knockdown of RSK4 abolished ΔNp63α-enhanced sphere formation ability, whereas RSK4 overexpression partially restored the effects of ΔNp63-suppressed sphere formation (n = 3 independent experiments). Scale bars, 100 μm. (B) Flow cytometry analysis of ALDH activity and the proportion of $CD90^+$ cells in ESCC cells from the indicated groups (n = 3 independent experiments). (C) Western blot analysis of ESCC cancer stem cell markers in the indicated groups. (D) Clonogenic survival assays of ESCC cells in the indicated groups at irradiation doses of 0, 3 and 6 Gy (n = 3 independent experiments). (E) Relative caspase-3 activity 24 h after IR (10 Gy) of ESCC cells in the indicated groups (n = 3 independent experiments). (F) Western blot analysis of phosphorylated and total amounts of checkpoint proteins ATM and CHK2 from the indicated groups 1h after 10 Gy of IR. (G) ESCC cells from the indicated groups were treated with IR (10 Gy) and recultured under normal conditions for 1 and 6 h, then subjected to Western blot analysis with γ-H2AX antibody. The "0 h" indicates cells with IR treatment but with no time for DNA repair. Data are representative of means ± SD. $^{**}P < 0.01$, $^{***}P < 0.001$. Differences were tested using unpaired 2-sided Student's t test (A, B, D, E).

Figure 6

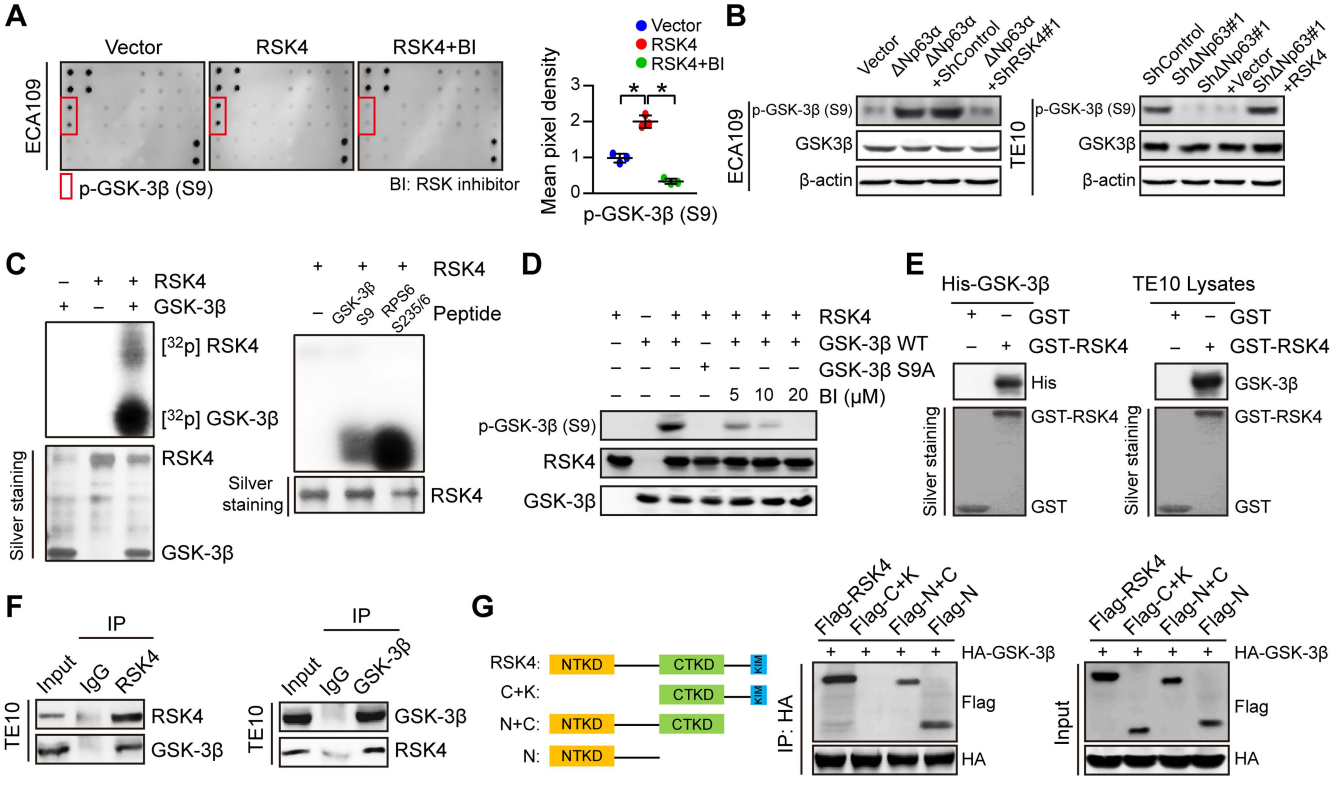
A
Vector
RSK4
RSK4+BI
ECA109
p-GSK-3β (S9)
BI: RSK inhibitor
Vector
RSK4
RSK4+BI
Mean pixel density
p-GSK-3β (S9)
B
Vector
ΔNp63α
ΔNp63α +ShControl
ΔNp63α +ShRSK4#1
ECA109
p-GSK-3β (S9)
GSK3β
β-actin
ShControl
ShΔNp63#1
ShΔNp63#1 +Vector
ShΔNp63#1 +RSK4
TE10
C
RSK4
GSK-3β
[32p] RSK4
[32p] GSK-3β
Silver staining
RSK4
GSK-3β
GSK-3β S9
RPS6 S235/6
Peptide
Silver staining
D
RSK4
GSK-3β WT
GSK-3β S9A
BI (μM)
p-GSK-3β (S9)
RSK4
GSK-3β
E
His-GSK-3β
TE10 Lysates
GST
GST-RSK4
His
GSK-3β
Silver staining
F
IP
Input
IgG
RSK4
GSK-3β
TE10
G
RSK4:
C+K:
N+C:
N:
NTKD
CTKD
KM
Flag-RSK4
Flag-C+K
Flag-N+C
Flag-N
HA-GSK-3β
IP: HA
Flag
HA
Input

Figure 6. RSK4 directly phosphorylates GSK-3β Ser9. (A) Mitogen-activated protein kinase (MAPK) pathway phosphor-antibody microarray analysis showing that phosphorylated GSK-3β Ser9 was significantly increased when RSK4 was stably overexpressed and decreased when treated with BI-D1870 (an inhibitor of RSK; 10 μM) for 12 h (n = 3 independent experiments). (B) Western blot analysis showing that downregulation of RSK4 resulted in a reduced level of ΔNp63α-induced phosphorylation of GSK-3β Ser9 (left), whereas RSK4 overexpression partially reversed the reduction in the phosphorylation level through ΔNp63 knockdown (right). (C) Active RSK4 phosphorylated GSK-3β at Ser9 in vitro in the presence of [γ-^{32}P] ATP as visualized by an autoradiograph. The RPS6 Ser235/6 peptide was used as a positive control. The input was confirmed by silver staining. (D) Validation of the phosphorylation level of p-GSK-3β Ser9 in an in vitro kinase assay by Western blot. The phosphorylation level of GSK-3β was inhibited when treated with BI-D1870 for 2 h. Wild-type (WT) GSK-3β and mutant GSK-3β S9A were used as substrates for active RSK4. (E) In vitro glutathione S-transferase (GST) pulldown assay verifying the interaction of RSK4 with purified His-GSK-3β protein (left) or GSK-3β from TE10 cell lysates (right). Retrieved proteins were evaluated by immunoblotting. GST-only protein was used as a negative control. GST fusion proteins were confirmed by silver staining. (F) The interaction of RSK4 and GSK-3β was confirmed by endogenous coimmunoprecipitation (co-IP) assay in TE10 cells. Immunoglobulin G (IgG) served as a negative control. (G) Mapping analyses of full-length and truncated RSK4 with representative co-IP assays in HEK293T cells showing that the N-terminal kinase

domain (NTKD) of RSK4 was responsible for the interaction with GSK-3β. CTKD, C-terminal kinase domain; KIM, kinase interaction motif. Data are representative of means ± SD. *$P < 0.05$. Differences were tested using 1-way ANOVA with Tukey's post hoc test (A).

Figure 7

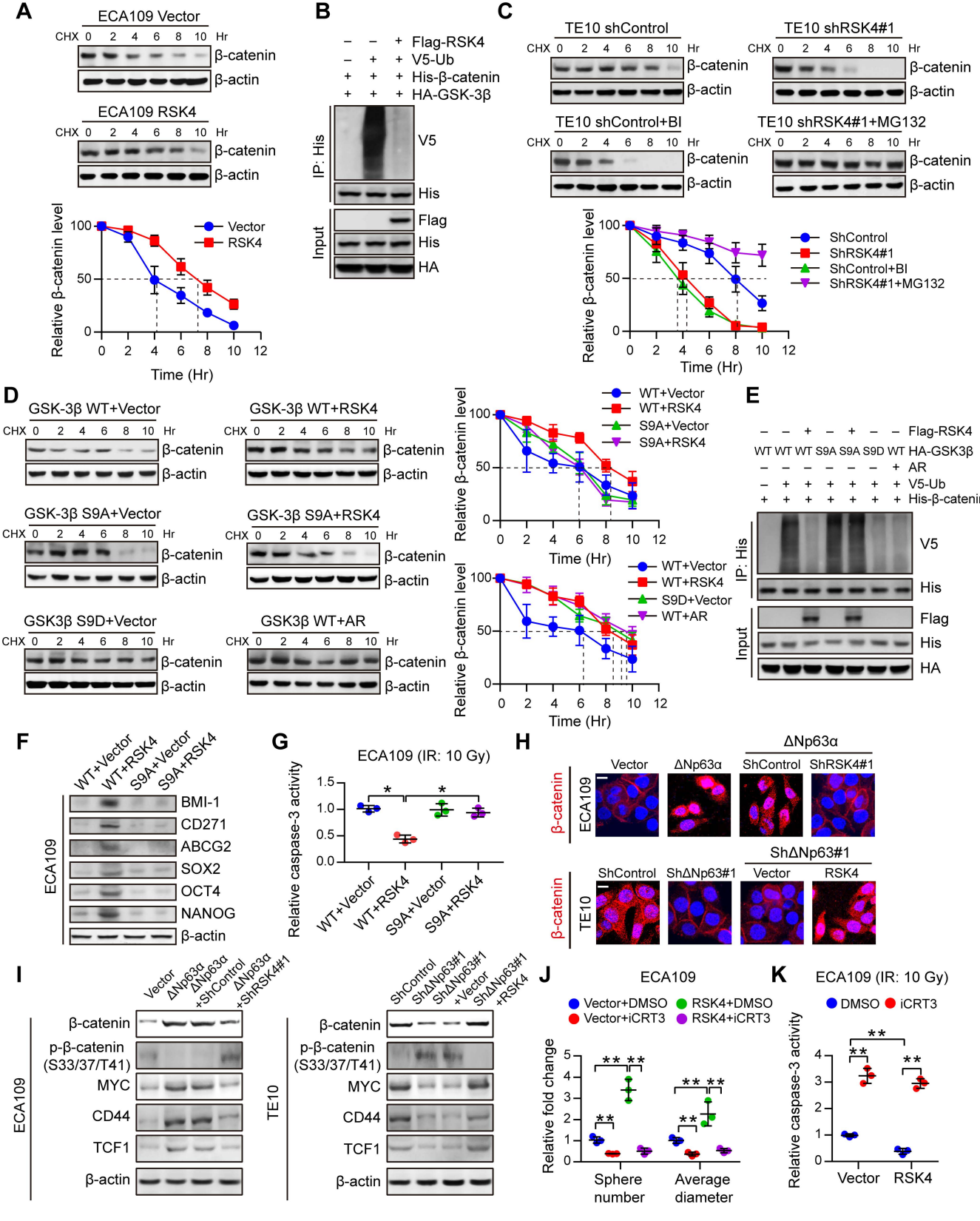
A
ECA109 Vector
CHX 0 2 4 6 8 10 Hr
β-catenin
β-actin
ECA109 RSK4
Relative β-catenin level
Vector
RSK4
Time (Hr)
B
Flag-RSK4
V5-Ub
His-β-catenin
HA-GSK-3β
IP: His
V5
His
Input
Flag
HA
C
TE10 shControl
TE10 shRSK4#1
TE10 shControl+BI
TE10 shRSK4#1+MG132
ShControl
ShRSK4#1
ShControl+BI
ShRSK4#1+MG132
D
GSK-3β WT+Vector
GSK-3β WT+RSK4
GSK-3β S9A+Vector
GSK-3β S9A+RSK4
GSK3β S9D+Vector
GSK3β WT+AR
WT+Vector
WT+RSK4
S9A+Vector
S9A+RSK4
S9D+Vector
WT+AR
E
WT WT WT S9A S9A S9D WT
AR
F
WT+Vector
WT+RSK4
S9A+Vector
S9A+RSK4
ECA109
BMI-1
CD271
ABCG2
SOX2
OCT4
NANOG
G
ECA109 (IR: 10 Gy)
Relative caspase-3 activity
H
ΔNp63α
Vector
ShControl
ShRSK4#1
ShΔNp63#1
RSK4
TE10
I
Vector
ΔNp63α
ΔNp63α +ShControl
ΔNp63α +ShRSK4#1
ShControl
ShΔNp63#1
ShΔNp63#1 +Vector
ShΔNp63#1 +RSK4
p-β-catenin (S33/37/T41)
MYC
CD44
TCF1
J
Vector+DMSO
Vector+iCRT3
RSK4+DMSO
RSK4+iCRT3
Relative fold change
Sphere number
Average diameter
K
DMSO
iCRT3

Figure 7. RSK4 activates the Wnt/β-catenin pathway. (A) Control or RSK4-overexpressing ECA109 cells were incubated with cycloheximide (CHX) (10 μg/mL) for the indicated times. High RSK4 expression prolonged the half-life of β-catenin degradation (n = 3 independent experiments). (B) HEK293T cells were transfected with the indicated plasmids, and cell extracts were IP with an anti-His antibody. Ubiquitinated β-catenin was detected by immunoblotting. (C) Control or RSK4-silenced TE10 cells were incubated with CHX (10 μg/mL), CHX plus BI-D1870 (10 μM), or MG132 (10 μM) for the indicated times. The indicated proteins were detected by immunoblotting (n = 3 independent experiments). (D) HEK293T cells were transfected with the indicated plasmids and incubated with CHX (10 μg/mL) for the indicated times. The indicated proteins were detected by immunoblotting (n = 3 independent experiments). (E) HEK293T cells were transfected with the indicated plasmids, and cell extracts were IP with an anti-His antibody. Ubiquitinated β-catenin was detected by immunoblotting. (F, G) ECA109 cells were transfected with the indicated plasmids, and then cancer stem cell markers (F) and caspase-3 activity after 10 Gy IR (G) of the indicated groups were detected (n = 3 independent experiments). (H) Representative image of the nuclear localization of β-catenin in ESCC cells from the indicated groups detected using immunofluorescence microscopy. Scale bars, 100 μm. (I) Effects of knockdown or overexpression of RSK4 on the indicated proteins in ΔNp63α-overexpressing or ΔNp63-suppressing ESCC cells. (J, K) Treatment of RSK4-overexpressing cells with iCRT3 (an inhibitor of β-catenin signaling; 50 μM) for 24 h greatly reduced their sphere formation ability (J) and increased caspase-3 activity after

IR (K) (n = 3 independent experiments). BI, BI-D1870; AR, AR-A014418. Data are representative of means ± SD. *$P < 0.05$, **$P < 0.01$. Differences were tested using 1-way ANOVA with Tukey's post hoc test (G, J, K).

Figure 8

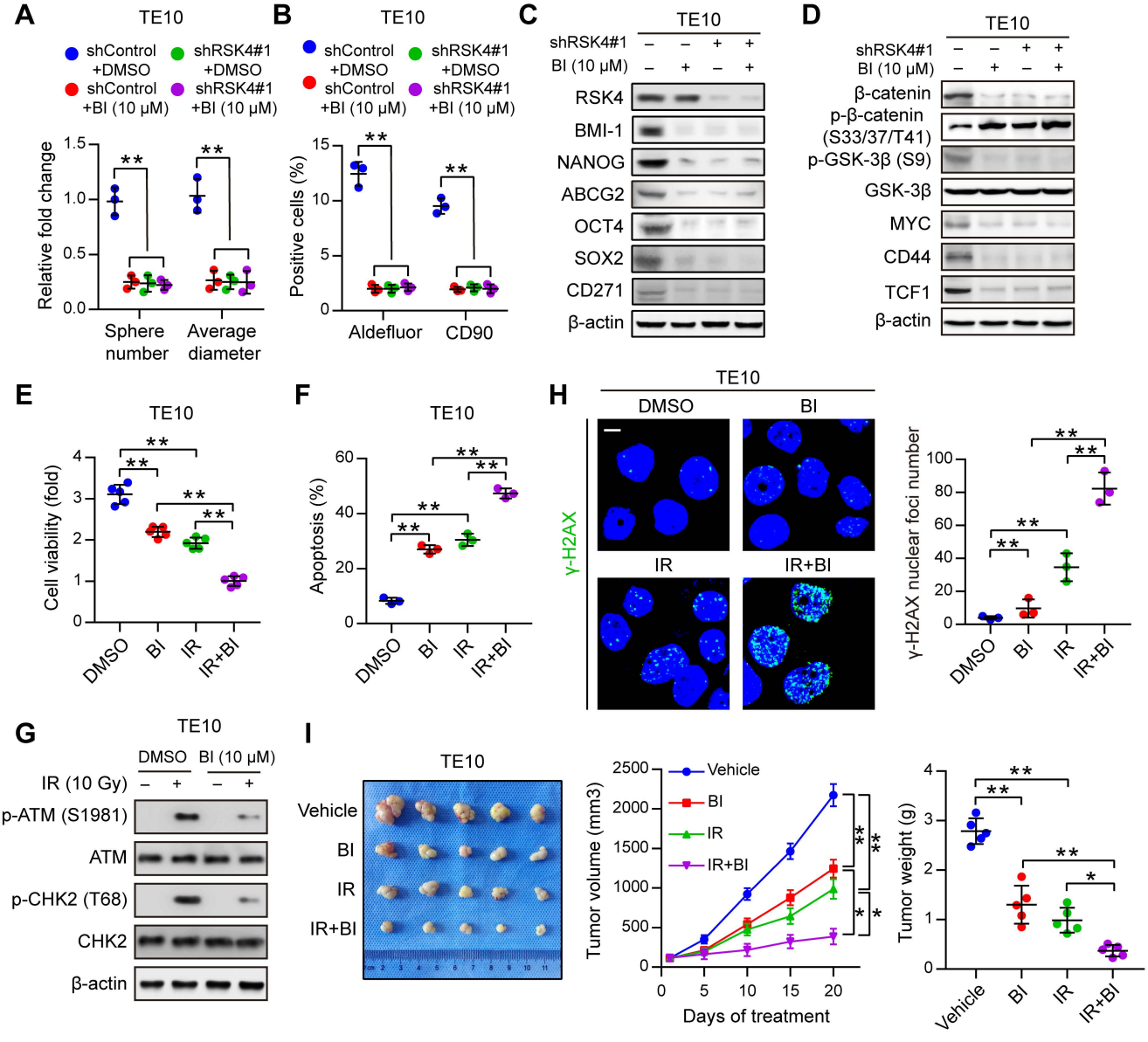
A
TE10
shControl +DMSO
shRSK4#1 +DMSO
shControl +BI (10 μM)
shRSK4#1 +BI (10 μM)
Relative fold change
Sphere number
Average diameter
B
TE10
Positive cells (%)
Aldefluor
CD90
C
TE10
shRSK4#1
BI (10 μM)
RSK4
BMI-1
NANOG
ABCG2
OCT4
SOX2
CD271
β-actin
D
TE10
shRSK4#1
BI (10 μM)
β-catenin
p-β-catenin (S33/37/T41)
p-GSK-3β (S9)
GSK-3β
MYC
CD44
TCF1
β-actin
E
TE10
Cell viability (fold)
DMSO
BI
IR
IR+BI
F
TE10
Apoptosis (%)
H
TE10
DMSO
BI
IR
IR+BI
γ-H2AX
γ-H2AX nuclear foci number
G
TE10
DMSO
BI (10 μM)
IR (10 Gy)
p-ATM (S1981)
ATM
p-CHK2 (T68)
CHK2
β-actin
I
TE10
Vehicle
BI
IR
IR+BI
Tumor volume (mm3)
Days of treatment
Tumor weight (g)

Figure 8. Disrupting the RSK4 pathway reduces the CSC properties and improves the radiosensitivity of ESCC. (A, B) Sphere formation assay (A) and flow cytometry analysis (B) of TE10 cells treated with BI-D1870 (10 μM), RSK4 knockdown or both (n = 3 independent experiments). (C) Immunoblot analyses of BMI-1, NANOG, ABCG2, OCT4, SOX2, and CD271 in TE10 cells with the indicated treatments. (D) Immunoblot analyses of β-catenin, p-β-catenin (S33/37/T41, inactive state), p-GSK-3β (S9), GSK-3β, MYC, CD44 and TCF1 in TE10 cells with the indicated treatments. (E) Cell viability assay of TE10 cells treated with BI-D1870 (10 μM) for 12 h, IR (10 Gy) or both (n = 3 independent experiments). (F) Fluorescence-activated cell sorting analyses of apoptosis of TE10 cells treated with BI-D1870 (10 μM) for 12 h, IR (10 Gy) or both (n = 3 independent experiments). (G) Western blot analysis of phosphorylated and total amounts of checkpoint proteins ATM and CHK2 from TE10 cells treated with or without BI-D1870 (10 μM) before treatment (-) and 1h after 10 Gy of IR (+). (H) Immunofluorescent staining of γ-H2AX in TE10 cells with the indicated treatments (n = 3 independent experiments). Scale bars, 100 μm. (I) ESCC-derived xenografts in mice treated with the vehicle control, BI-D1870 (50 mg/kg per day, intraperitoneal injection), and/or IR (5 Gy×2 times). The growth curve of tumor size and the average tumor weight are presented (5 mice each). Data are representative of means ± SD. $*P < 0.05$, $**P < 0.01$. Differences were tested using 1-way ANOVA with Tukey's post hoc test (A, B, E, F, H, I).

Figure 9

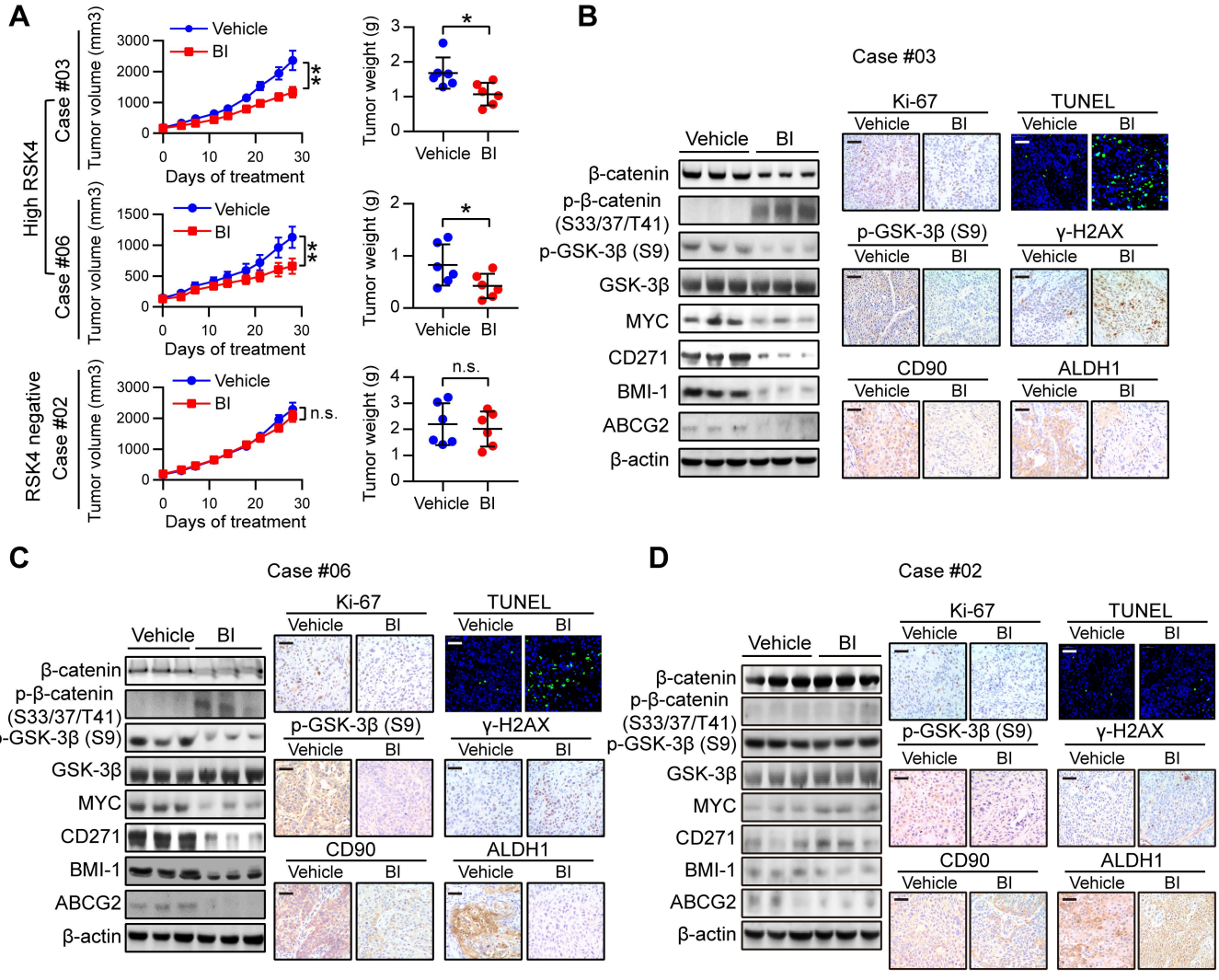
A
High RSK4
Case #03
Case #06
RSK4 negative
Case #02
Tumor volume (mm3)
Vehicle
BI
Days of treatment
Tumor weight (g)
n.s.
B
Case #03
Vehicle
BI
β-catenin
p-β-catenin (S33/37/T41)
p-GSK-3β (S9)
GSK-3β
MYC
CD271
BMI-1
ABCG2
β-actin
Ki-67
TUNEL
p-GSK-3β (S9)
γ-H2AX
CD90
ALDH1
C
Case #06
D
Case #02

Figure 9. BI-D1870 inhibits tumor growth in ESCC patient-derived xenografts. (A) Tumor volume growth curve and tumor weight of patient-derived xenograft (PDX) mice with different RSK4 expression levels treated with BI-D1870 (50 mg/kg per day, intraperitoneal injection) or the vehicle for 28 days (6 mice each). (B-D) Immunoblot, immunohistochemistry and terminal deoxynucleotidyl transferase-mediated dUTP labeling (TUNEL) analyses of the indicated markers in PDX tumors #03 (B), #06 (C) and #02 (D) treated with BI-D1870 (50 mg/kg per day, intraperitoneal injection) or the vehicle. Scale bars, 100 μm. n.s., not significant. Data are representative of means ± SD. *$P < 0.05$, **$P < 0.01$. Differences were tested using unpaired 2-sided Student's t test (A).

Figure 10

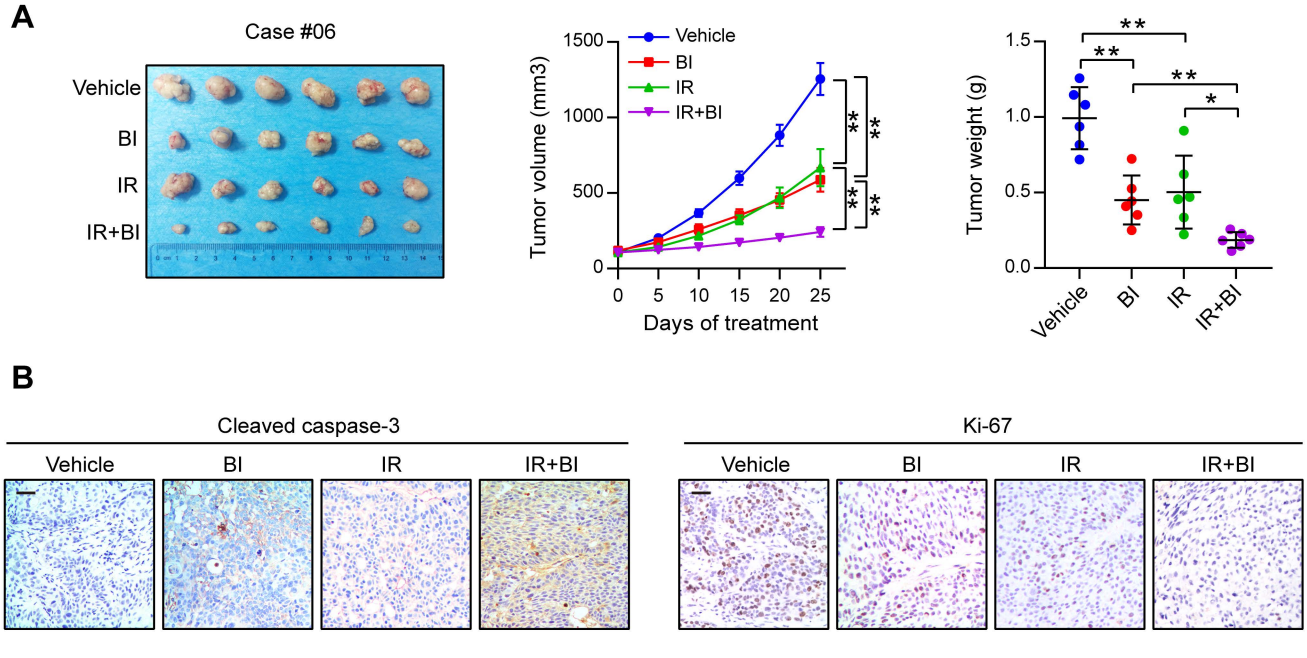
A
Case #06
Vehicle
BI
IR
IR+BI
Tumor volume (mm3)
Days of treatment
Tumor weight (g)
B
Cleaved caspase-3
Ki-67
Vehicle
BI
IR
IR+BI

Figure 10. BI-D1870 improves the therapeutic efficacy of radiotherapy in ESCC patient-derived xenografts. (A) PDX tumor #06 treated with the vehicle control, BI-D1870 (50 mg/kg per day, intraperitoneal injection), and/or IR (5 Gy×2 times). The growth curve of tumor size and the average tumor weight are presented (6 mice each). (B) IHC analyses of cleaved caspase-3 and Ki-67 in the indicated groups. Scale bars, 100 μm. Data are representative of means ± SD. **P* < 0.05, ***P* < 0.01. Differences were tested using 1-way ANOVA with Tukey's post hoc test (A).